

RESEARCH ARTICLE

MK3 Modulation Affects BMI1-Dependent and Independent Cell Cycle Check-Points

Peggy Prickaerts¹, Hanneke E. C. Niessen¹, Vivian E. H. Dahlmans¹, Frank Spaapen¹, Juliette Salvaing^{1^{‡a}}, Jolien Vanhove^{1^{‡b}}, Claudia Geijselaers¹, Stefanie J. J. Bartels^{1^{‡c}}, Iris Partouns¹, Dietbert Neumann¹, Ernst-Jan Speel², Yoshihiro Takihara³, Bradly G. Wouters⁴, Jan Willem Voncken^{1*}

1 Department of Molecular Genetics, Maastricht University Medical Centre, Maastricht, the Netherlands, **2** Department of Pathology, Maastricht University Medical Centre, Maastricht, the Netherlands, **3** Department of Stem Cell Biology, Research Institute for Radiation Biology and Medicine, Hiroshima University, Hiroshima, Japan, **4** Princess Margaret Cancer Centre and Campbell Family Institute for Cancer Research, Departments of Radiation Oncology and Medical Biophysics, University Health Network, Toronto, Canada, Maastricht Radiation Oncology (MaastRO) Lab, Maastricht University, Maastricht, The Netherlands

☞ These authors contributed equally to this work.

‡a Current address: INRA, Biologie du Développement et Reproduction, Jouy-en-Josas, France

‡b Current address: Department of Development and Regeneration, Interdepartmental Stem Cell Institute Leuven (SCIL), Catholic Universiteit Leuven, Leuven, Belgium

‡c Current address: Department of Molecular Biology, Nijmegen Centre for Molecular Life Sciences, Radboud University, Nijmegen, The Netherlands

* w.voncken@maastrichtuniversity.nl



OPEN ACCESS

Citation: Prickaerts P, Niessen HEC, Dahlmans VEH, Spaapen F, Salvaing J, Vanhove J, et al. (2015) MK3 Modulation Affects BMI1-Dependent and Independent Cell Cycle Check-Points. PLoS ONE 10 (4): e0118840. doi:10.1371/journal.pone.0118840

Academic Editor: Gilbert Bernier, University of Montréal and Hôpital Maisonneuve-Rosemont, CANADA

Received: November 4, 2013

Accepted: January 14, 2015

Published: April 8, 2015

Copyright: © 2015 Prickaerts et al. This is an open access article distributed under the terms of the [Creative Commons Attribution License](https://creativecommons.org/licenses/by/4.0/), which permits unrestricted use, distribution, and reproduction in any medium, provided the original author and source are credited.

Funding: Netherlands organization for Scientific Research (ZonMW-NWO): Research Support grant 908-02-040 (JWV), VIDI grant 016.046.362 (JWV); transnational University Limburg grant (JWV, BGW); Netherlands Genome Initiative (NGI) fellowship 050-72-422 (HN) and EMBO fellowship (HN). Netherlands Organization for Scientific Research (ZonMW-NWO): VIDI grant 864.10.007 (DN). The funders had no role in study design, data collection and analysis, decision to publish, or preparation of the manuscript.

Competing Interests: The authors have declared that no competing interests exist.

Abstract

Although the MK3 gene was originally found deleted in some cancers, it is highly expressed in others. The relevance of MK3 for oncogenesis is currently not clear. We recently reported that MK3 controls ERK activity via a negative feedback mechanism. This prompted us to investigate a potential role for MK3 in cell proliferation. We here show that overexpression of MK3 induces a proliferative arrest in normal diploid human fibroblasts, characterized by enhanced expression of replication stress- and senescence-associated markers. Surprisingly, MK3 depletion evokes similar senescence characteristics in the fibroblast model. We previously identified MK3 as a binding partner of Polycomb Repressive Complex 1 (PRC1) proteins. In the current study we show that MK3 overexpression results in reduced cellular EZH2 levels and concomitant loss of epigenetic H3K27me3-marking and PRC1/chromatin-occupation at the *CDKN2A/INK4A* locus. In agreement with this, the PRC1 oncoprotein BMI1, but not the PCR2 protein EZH2, bypasses MK3-induced senescence in fibroblasts and suppresses P16^{INK4A} expression. In contrast, BMI1 does not rescue the MK3 loss-of-function phenotype, suggesting the involvement of multiple different checkpoints in gain and loss of MK3 function. Notably, MK3 ablation enhances proliferation in two different cancer cells. Finally, the fibroblast model was used to evaluate the effect of potential tumorigenic MK3 driver-mutations on cell proliferation and M/SAPK signaling imbalance. Taken together, our findings support a role for MK3 in control of proliferation and replicative life-span, in part through concerted action with BMI1, and suggest that the effect of MK3 modulation or mutation on M/SAPK signaling and, ultimately, proliferation, is cell context-dependent.

Introduction

Sequential activation of kinases within the canonical M/SAPK (mitogen/stress activated protein kinase) cascades is a common and evolutionary-conserved signal transduction mechanism. The canonical M/SAPK cascades cooperate in transmitting and integrating intra- and extracellular signals, thereby controlling a large number of, sometimes opposing, cellular processes such as proliferation, differentiation, survival, stress response, and apoptosis [1]. Downstream of M/SAPKs, MAPK-activated protein kinases (MAPKAPKs), including RSK1-4, MSK1/2, MNK1/2 and MK2/3/5, signal to diverse cellular targets. Among the MAPKAPKs are three structurally related MKs MK2, MK3 and MK5. Despite their high homology, the three MKs display distinct spatio-temporal expression profiles and act in different biological processes [2,3]. Identification of MK-substrates suggests that MKs function in numerous cellular processes, including gene transcription, mRNA-stability and translation, cytoskeleton remodeling, cell proliferation and apoptosis. Besides their joint involvement in inflammatory responses, the biological relevance of substrate interaction and phosphorylation by MKs remains largely unclear.

MK3 (MAPKAPK3, 3pK) was identified as the first MK activated down-stream of all three mitogen- and stress-activated protein kinase (M/SAPK) cascades; consequentially, MK3 was considered an integration point of converging mitogenic and stress signaling [4]. Whereas the RAS-M/SAPK signalling pathways have a long-standing link to cancer, the involvement of MKs in cancer is currently unclear. MK3, originally referred to as 3pK (chromosome 3p kinase), was found frequently homozygously deleted as part of the 3p21.3 region in small cell lung cancer and other cancers and cancer cell lines [5,6]. Conversely, potential oncogenic 'driver' mutations have been identified in MK3 [7]. These records point to an involvement of MK3 in tumorigenesis and support the idea that it may act tumorigenic or tumor-suppressive.

We previously reported that MK3 associates with PRC1-complexes through direct SAM (Self-Association Motif) domain-mediated interaction with the *Polyhomeotic* orthologs PHC1 and PHC2 [8]. Polycomb Group repressive complexes (PRC1 and PRC2) act as part of a cellular epigenetic memory system and play an important role in the determination of cell fate [9]. Both core complexes harbor intrinsic PRC protein-associated epigenetic catalytic activity, and are known to interact with additional epigenetic regulators. These interactions and catalytic activities are controlled by post-translational modification [10,11]. In addition, we established that phosphorylation of the PRC1 complex controls PRC1/chromatin-association [8,12]. PRC proteins have been linked to oncogenesis: high expression or mutation of several PRC members has been etiologically implicated in the onset and malignant progression of cancer [13].

Recent data from our group identified MK3 as a regulator of the PRC1 target gene ATF3-expression via a negative feedback mechanisms on MEK1 and ERK1/2 in the context of mitogenic stimulation. We found that MK3 ablation or inhibition resulted in prolonged ERK phosphorylation and increased ATF3 and premature and elevated EGR1 expression [14]. Using a genetic *Drosophila* model for wing development, we confirmed exaggerated mitogenic ERK-signaling in the absence of dMK (the only *Drosophila* MK ortholog), thus supporting a negative regulatory role for MK3 in canonical ERK signaling [14]. In addition, besides ERK, modulation of MK3 levels also affects cellular P38 and JNK protein levels [14,15]. Combined, these observations suggest that altered cellular MK3 levels and or activity may contribute to deregulation of cellular proliferation through deregulation of M/SAPK, potentially contributing to tumorigenesis.

In this study we tested the hypothesis that MK3 controls cell proliferation using MK3-gain- and loss-of-function constructs in normal and cancer cells. In addition, we aimed to investigate the biological relevance of the interaction between MK3 and PRC1 in the context of cell proliferation. We provide evidence for a genetic interaction between the Polycomb Group protein

BMI1 and MK3 in proliferative life span: BMI1 overcame the MK3-overexpression phenotype in normal cells. In contrast, BMI1 did not compensate for the negative effect of MK3 depletion on cell proliferation. MK3 overexpression inhibited the proliferation of normal and cancer cells. In contrast, MK3 depletion enhanced the cell cycling of cancer cell lines. Our data supports the idea that MK3-mediated abnormal M/SAPK signaling intersects with known checkpoints and contributes proliferative control. The potential implications of these observations for tumorigenesis are discussed.

Results

Gain or loss of MK3 function induces senescence in normal human fibroblasts

To study the role of MK3 in cellular processes related to cell proliferation, we modulated cellular MK3 levels in different cell models using retroviral expression systems and measured the effects thereof. We initially focused on normal diploid human TIG3 fibroblasts to determine the effect of forced overexpression of wild type (non-mutated) MK3 ($MK3^{WT}OE$) on cell proliferation (Fig 1A). Transduced TIG3 cells were expanded under selection pressure; proliferative capacity of these cultures was assessed at ± 1 week and ± 4 weeks after transduction. TIG3/ $MK3^{WT}OE$ displayed clearly decreased proliferative capacity relative to empty vector control cells at the early time point and had altogether stopped dividing at 4 weeks post-transduction (Fig 1B). By means of reference, TIG3/*Bmi1*OE maintained proliferative capacity throughout the duration of the experiment, whereas primary empty vector-transduced TIG3 (*con*) progressively lost proliferative capacity due to limited proliferative lifespan *in vitro* (Fig 1B). DNA-profiling at late time points post-transduction revealed an increased number of cells in G0/G1 at the expense of cells in S-phase upon MK3-overexpression (Fig 1C); overexpression of the *RASV12* oncogene reduced S-phase cell numbers as anticipated as *RASV12* is known to evoke oncogene-induced senescence (OIS) [16], Fig 1C). Reduced *de novo* DNA synthesis in TIG3/ $MK3^{WT}OE$ cells was confirmed by a markedly lower number of BrdU-positive cells in TIG3/ $MK3^{WT}OE$ cultures and (Figs 1D and S1A); equal relative distribution of cells throughout S-phase suggested that TIG3/ $MK3^{WT}OE$ cultures had undergone an intraS-phase arrest, a feature known to occur in the context of oncogene-induced senescence (OIS) (S1B Fig).

In further support of activation of a senescence-associated response by MK3, TIG3/ $MK3^{WT}OE$ cells displayed enlarged, flat-cell morphology (Fig 2A). The occurrence of senescence was further corroborated by expression of the senescence-associated beta-Galactosidase (SA-bGal) marker protein in large flat cells (Fig 2A). $MK3^{WT}$ -overexpression also negatively affected cell division in immortal TIG3^{hTERT} cells, indicating that MK3 acts downstream or independent of hTERT in proliferative control (S1C Fig). TP53 is a senescence marker, activated downstream of e.g. increased mitogenic signaling through RAS/ERK [17–20]. Consistent with the observed MK3-mediated senescence response, global expression of TP53 was elevated in TIG3/ $MK3^{WT}OE$ cells (Fig 2B). Increased staining of TP53 was readily detectable in senescent TIG3/ $MK3^{WT}OE$ nuclei (Fig 2C); likewise expression of P21^{CIP1/WAF1}, a direct transcriptional target of TP53, was increased (Fig 2B). The increased expression of P16^{INK4a} in relation to sustained $MK3^{WT}OE$ was consistent with its crucial role in establishing irreversible senescence (Fig 2B) [17,21,22]. We next tested whether the adverse effect of $MK3^{WT}OE$ was dependent on its kinase activity. Surprisingly, the early effect of $MK3^{WT}OE$ on cell proliferation occurred independent of MK3 kinase activity, as expression of a kinase-dead mutant ($MK3^{KM}OE$) and a constitutively active mutant ($MK3^{CA}OE$) did not affect cell proliferation at 1 week post-transduction (S2A Fig). In agreement with this, cellular TP53 levels were only moderately increased in the TIG3/ $MK3OE$ cells, not in TIG3/ $MK3^{KM}OE$ or TIG3/ $MK3^{CA}OE$ cells. P16^{INK4A} levels were substantially increased at 1 week post-transduction

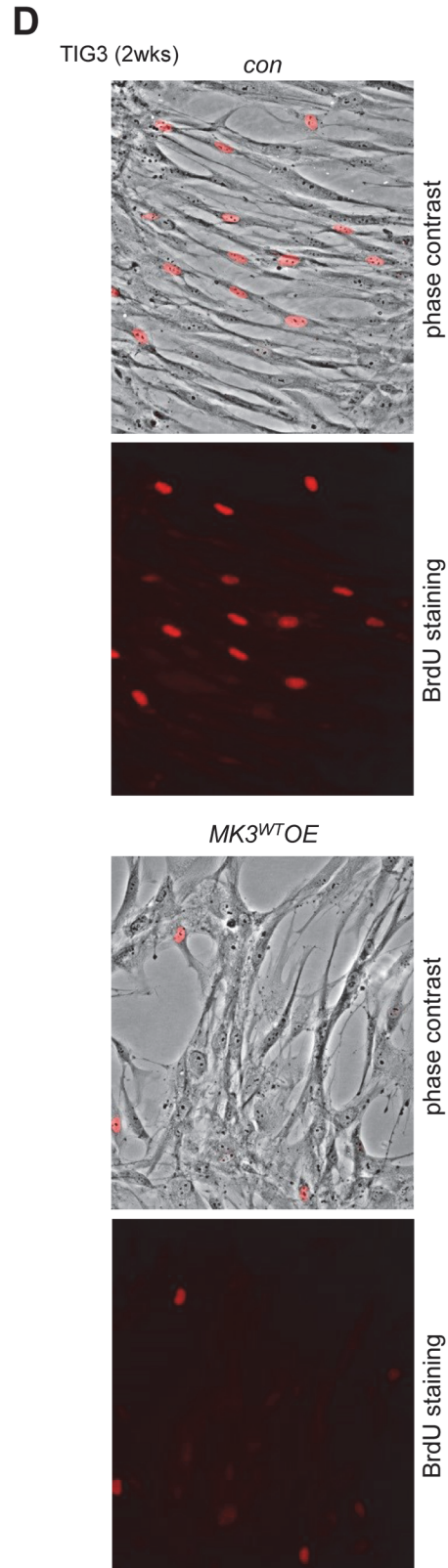
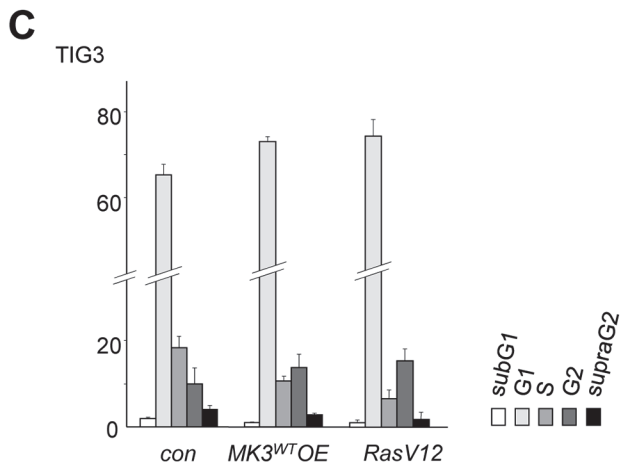
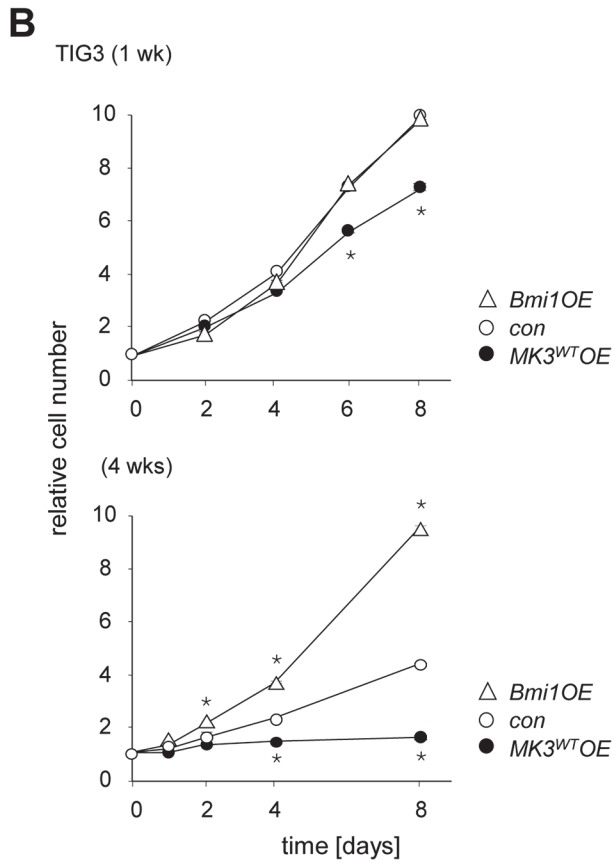
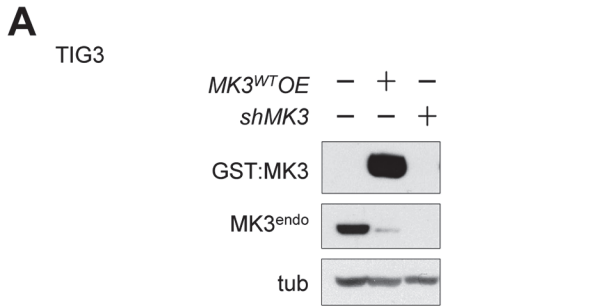


Fig 1. $MK3^{WT}$ overexpression induces a proliferative arrest in normal human fibroblasts. (A) Retroviral expression systems were applied to enhance ($MK3^{WT}OE$) or remove ($shMK3$) MK3 expression. Western blot shows MK3 proteins: endogenous ($MK3^{endo}$) and overexpressed (GST:MK3). (B) Proliferation curves of TIG3 cells transduced with: a retroviral $MK3$ expression vector ($MK3^{WT}OE$; filled circles), an empty vector (con; open circles) or a murine $Bmi1$ expression vector (open triangles); proliferation was determined at 1 week (top panel) or ± 4 weeks (bottom panel) after retroviral transduction of TIG3 cells. Cell counts at $t = 2$ through $t = 8$ were normalized to cell counts at $t = 0$ for each transduced cell culture individually (see [Methods](#) section for details); statistical significance was determined by two-tailed Student's t-test and is presented relative to the empty vector control (* $p < 0.05$). (C) Quantification of DNA profiles (BrdU pulse-labeling and S-phase quantification by FACS) in TIG3/ $MK3^{WT}OE$ cells at approximately 1 week post-transduction. $RasV12$ -transduced cells were used as a positive control. (D) $MK3^{WT}OE$ reduces *de novo* DNA synthesis in TIG3/ $MK3^{WT}OE$ cells; cell counts: control (con) 699 BrdU-positive cells/10 fields; $MK3^{WT}OE$: 442 BrdU-positive cells/9 fields.

doi:10.1371/journal.pone.0118840.g001

in both TIG3/ $MK3^{WT}OE$ and TIG3/ $MK3^{CA}OE$ cultures, despite the differences in proliferation rate ([S2A and S2B Fig](#)). $P16^{INK4A}$ was also induced by $MK3^{KM}OE$, however, at a lower level than in both other conditions. Despite the initial absence of adverse effects on proliferation, all three MK3 variants reduced proliferation rate at 4 weeks post-transduction ([S2A and S2B Fig](#)). The absence of correlation between TP53 and $P16^{INK4A}$ levels and proliferation rate at 4 weeks suggests a potential contribution of additional molecular targets and mechanisms to the observed effects on proliferation. Combined this data shows that overexpression of $MK3^{WT}$ or two MK3 kinase mutants in human diploid fibroblasts reduces their proliferative capacity.

As the $MK3$ locus is frequently missing in cancers as part of often larger genomic deletions [[5,6](#)], it is conceivable that cellular MK3 depletion affects cell cycle regulation and contributes to tumorigenesis. To study the effect of loss of MK3 on cell proliferation, we next reduced cellular MK3 levels using RNA-interference. To this end a retroviral $shRNA$ construct was designed that selectively targeted $MK3$ ($shMK3$) ([S2C Fig](#); cf. [Fig 1A](#)). Similar to $MK3$ overexpression in TIG3 cells, $MK3$ depletion resulted in reduced proliferation of TIG3/ $shMK3$ cells and increased flat cell formation ([Fig 2D](#)), which was confirmed by reduced BrdU-incorporation in TIG3/ $shMK3$ cultures ([S2D Fig](#)). The $shMK3$ -associated arrest in normal cells was accompanied by increased TP53, $P21^{CIP1/WAF1}$ and $P16^{INK4A}$ expression ([Fig 2E](#)). As $MK2$ is also expressed in TIG3 cells (cf. [S5B Fig](#)) we aimed to exclude the possibility that $MK2$ confounded the observed $MK3$ depletion-associated proliferative phenotype. To this end TIG3 cells were either transduced with a $shMK3$ or a $shMK2/3$ construct; the latter effectively reduced expression of both $MK2$ and $MK3$ ([S2C Fig](#)). Both constructs increased G1-arrest with equal efficiency; $MK2$ neither compensated for loss of $MK3$ nor added to the effect of $MK3$ depletion, suggesting that the observed proliferative reduction could be attributed to $MK3$ in this experimental setting ([S2E Fig](#)). Thus, overexpression as well as depletion of $MK3$ in TIG3 cells induced a proliferative block, which correlated with expression of known senescence markers. Taken together, these results suggested that $MK3$ controls proliferative lifespan in normal diploid human fibroblasts.

Genetic interaction between MK3 and Polycomb in proliferative lifespan

$MK3$ has been identified as a PRC1 binding partner; we have shown that signaling through ERK1/2, P38 and $MK3$ controls gene expression via modulating chromatin-association of the PRC1 complex [[8,14](#)]. We further explored the functional interaction between PRC-function and $MK3$ in the context of cell proliferation. Senescent cells are known to release $CDKN2A/INK4A$ repression and show increased $P16^{INK4A}$ and/or $P14^{ARF}$ levels [[22–24](#)]. Increased expression at the $CDKN2A$ locus correlates with reduced local H3K27me3 [[25,26](#)]. Expression of the responsible histone H3K27 methyltransferase (HMT), the PRC2-class protein EZH2, was reported to be progressively reduced by TP53 in senescing cells [[27,28](#)]. Transcriptional repression of the $CDKN2A$ -locus in proliferating cells correlates with PRC2-mediated histone H3 Lysine 27 trimethylation (H3K27me3) [[25,26](#)]. In good agreement with these reports, we observed that global TP53 and EZH2 protein levels inversely correlated in senescent TIG3/ $MK3^{WT}OE$ cultures and

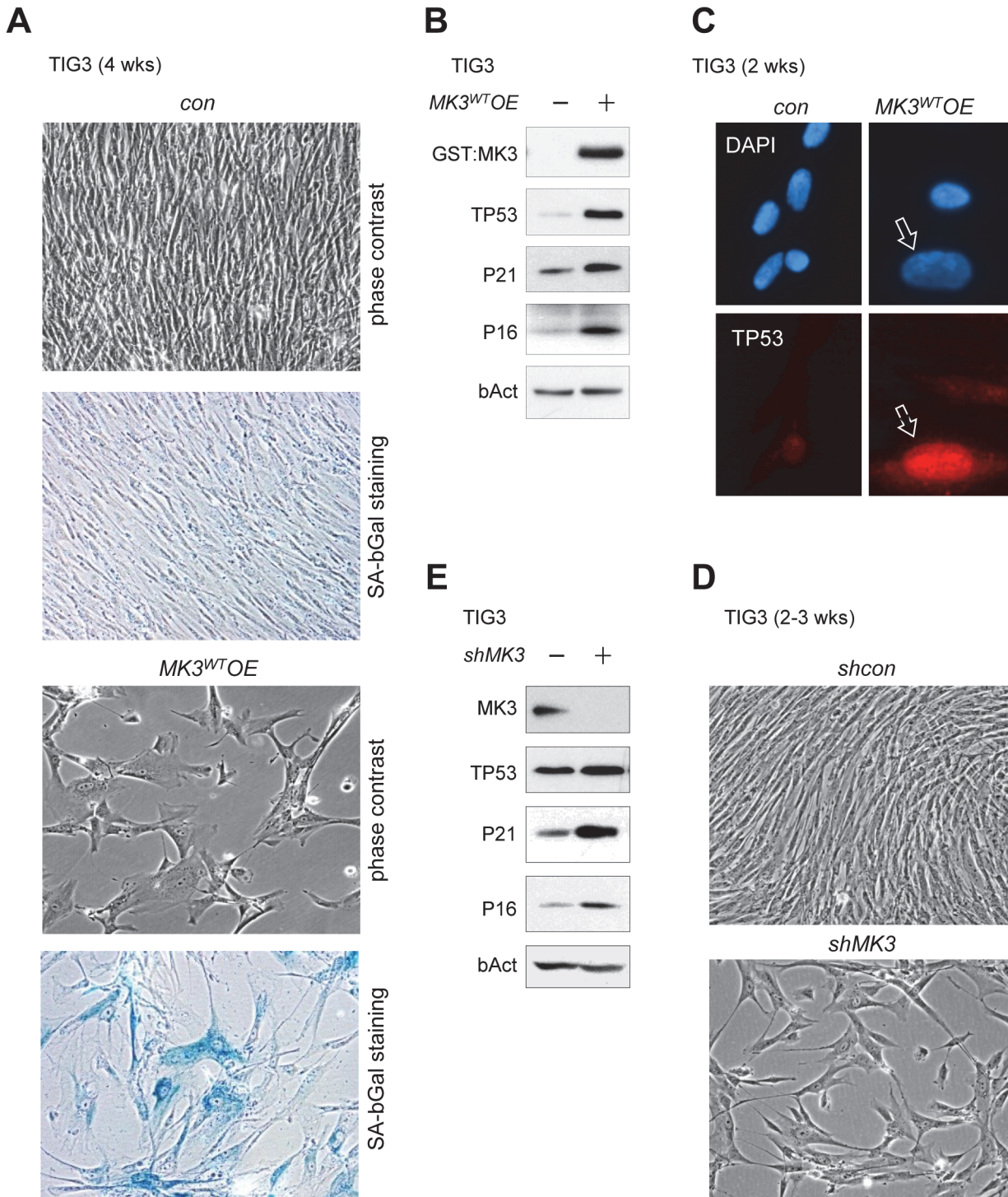


Fig 2. The *MK3^{WT}OE*-induced proliferative block in normal cells correlates with induction of known senescence markers. (A) Cell morphology in TIG3/*MK3^{WT}OE* cells (phase contrast; right upper panel); senescence-associated beta-Galactosidase (SA-bGal) staining in TIG3/*MK3^{WT}OE* cells (right lower panel). (B) Protein expression levels of MK3, TP53, P21^{CIP1/WAF1} (P21) and P16^{INK4A} (P16) in TIG3/*MK3^{WT}OE* (*MK3^{WT}OE*) versus control (*con*) cell lysates; loading control: b-Actin (bAct). TIG3/*MK3^{WT}OE* cells were cultured for approximately 3–4 weeks prior to extraction. (C) Nuclear TP53 accumulation in senescent TIG3/*MK3^{WT}OE* cells; counterstaining: DAPI. (D) Phase contrast images showing cello morphology in TIG3/*shMK3* cells (*shMK3*, lower panel; phase contrast) versus control cells (*shcon*; upper panel). Retrovirally transduced TIG3 cells (*shcon* and *shMK3*) were submitted to puromycin selection for 3–4 days, and plated at equal density (20–25% confluency) at the onset of the experiment; pictures were taken when *shcon* cells reached confluency. (E) Analysis of protein expression in TIG3/*shMK3* and control (*shcon*) cell lysates: TP53, P21^{CIP1/WAF1} (P21) and P16^{INK4A} (P16); loading control: b-Actin (bAct).

doi:10.1371/journal.pone.0118840.g002

that reduced cellular EZH2 correlated with increased $P16^{INK4A}$ expression (Fig 3A; cf. Fig 2B). Reduced EZH2 levels also inversely correlated with $P16^{INK4A}$ expression in senescent TIG3/*shMK3* cultures (Fig 3B), in further support of a functional link between EZH2 reduction and senescence upon modulation of MK3 levels. In addition to EZH2, CBX8 levels were reduced in both senescent TIG3/ $MK3^{WT}OE$ and TIG3/*shMK3* cultures, whereas PHC1 levels appeared relatively unaffected by gain or loss of MK3 function (Fig 3A and 3B). Thus far, the combined data shows that MK3 modulation induces a state of senescence that correlates with reduced cellular EZH2 levels and elevated $P16^{INK4A}$ expression.

To assess changes in PRC1 protein/chromatin-association and Polycomb-related status at the *CDKN2A/INK4A* locus in relation to MK3 overexpression, we applied chromatin immunoprecipitation (ChIP) technology to pre-senescent TIG3/ $MK3^{WT}OE$ cell cultures. The *CDKN2A/INK4A* locus has been mapped before in detail in regards to H3K27me3-marking and PRC1-occupation in proliferating and senescent cells [25,26]. A number of previously identified PRC1-negative (*p15exon1*; *p14exon1*) and positive (*HOXA10*; *HOXA11*) regions were used as controls in our analyses [25]. MK3-overexpression moderately, but consistently enhanced chromatin-occupation of MK3 at all loci probed including non-PRC1 target loci (Fig 3C), in line with our earlier observation that part of cellular MK3 associates with chromatin [8]. Absence or presence of H3K27me3-marking in our experimental model correlated perfectly with absence or presence of CBX8 occupation, respectively (Fig 3C); CBX8 binds the K27 trimethyl-mark through its chromobox domain [25,29]. Interestingly, chromatin-occupation of PHC1, a direct binding partner of MK3 [8], increased in parallel with MK3 at all promoter sequences analyzed, including at non-PRC1 target loci (Fig 3C). In contrast to CBX8, PHC1 was found associated also with non-PRC1 target loci, suggesting that (part of) PHC1 may associate with chromatin in an H3K27me3-independent fashion (Fig 3C). Relevantly, MK3-associated induction of senescence correlated with loss of H3K27me3-enrichment at *p16-exon1* and CBX8-displacement from the $P16^{INK4A}$ locus (promoter and exon1; Fig 3C). This data is in good agreement with both the reduced cellular EZH2 and CBX8 levels, and with the increased $P16^{INK4A}$ expression (S3B Fig) [25,26]. Combined, this data shows that in the $MK3^{WT}$ -overexpressed state, cellular senescence correlates with reduced cellular EZH2 and CBX8 levels and consequential de-repression of transcription at the *CDKN2A* locus.

We next explored the functional relationship between MK3 and BMI1 in proliferative lifespan. Genetic ablation of PRC1-members, among which BMI1 and PHC paralogs, is known to induce premature cellular senescence *in vitro* and *in vivo* [30,31]. In the light of the herein described local (*i.e.* at the *CDKN2A* locus) chromatin-displacement of PRC1 in senescing cells and our previous observation that prolonged *MK3* overexpression leads to reduction of chromatin-associated BMI1 [8], we speculated that *Bmi1OE* would overcome the senescent state induced by gain or loss of MK3 function. To determine whether *Bmi1OE* could bypass the negative effect of *MK3OE* on proliferative capacity, TIG3 fibroblasts were sequentially transduced with murine *Bmi1* and *MK3*-encoding retroviral expression vectors. *Bmi1OE* consistently produced a proliferative advantage for TIG3 fibroblasts (TIG3/*Bmi1OE/MK3^{WT}OE*) (Fig 4A and 4B). Whereas $MK3^{WT}$ overexpression alone reproducibly showed reduced TIG3 proliferation, co-expression of *Bmi1* compensated for the adverse effects of $MK3^{WT}$ overexpression on cell proliferation (Fig 4A). Importantly, in contrast to $MK3^{WT}$ expression, the adverse effect of MK3 ablation on fibroblast proliferation was not rescued by BMI1 (Fig 4B). *Bmi1* co-expression also reversed the MK3-induced senescent cell morphology in observed in TIG3/ $MK3^{WT}OE$ cultures, (Fig 4C). Co-expression of *Bmi1* in TIG3/ $MK3^{WT}OE$ cells prevented loss of EZH2 as well as of the PRC1 complex proteins CBX4 and RNF2 (Fig 4D). Finally, the global increase of H3K27me3 observed in TIG3/ $MK3^{WT}OE$ cells was prevented by co-expression of *Bmi1* (Fig 4D). TP53 expression in TIG3/ $MK3^{WT}OE$ cells was countered by BMI1 co-expression (Fig 4E). Relevantly, sequentially

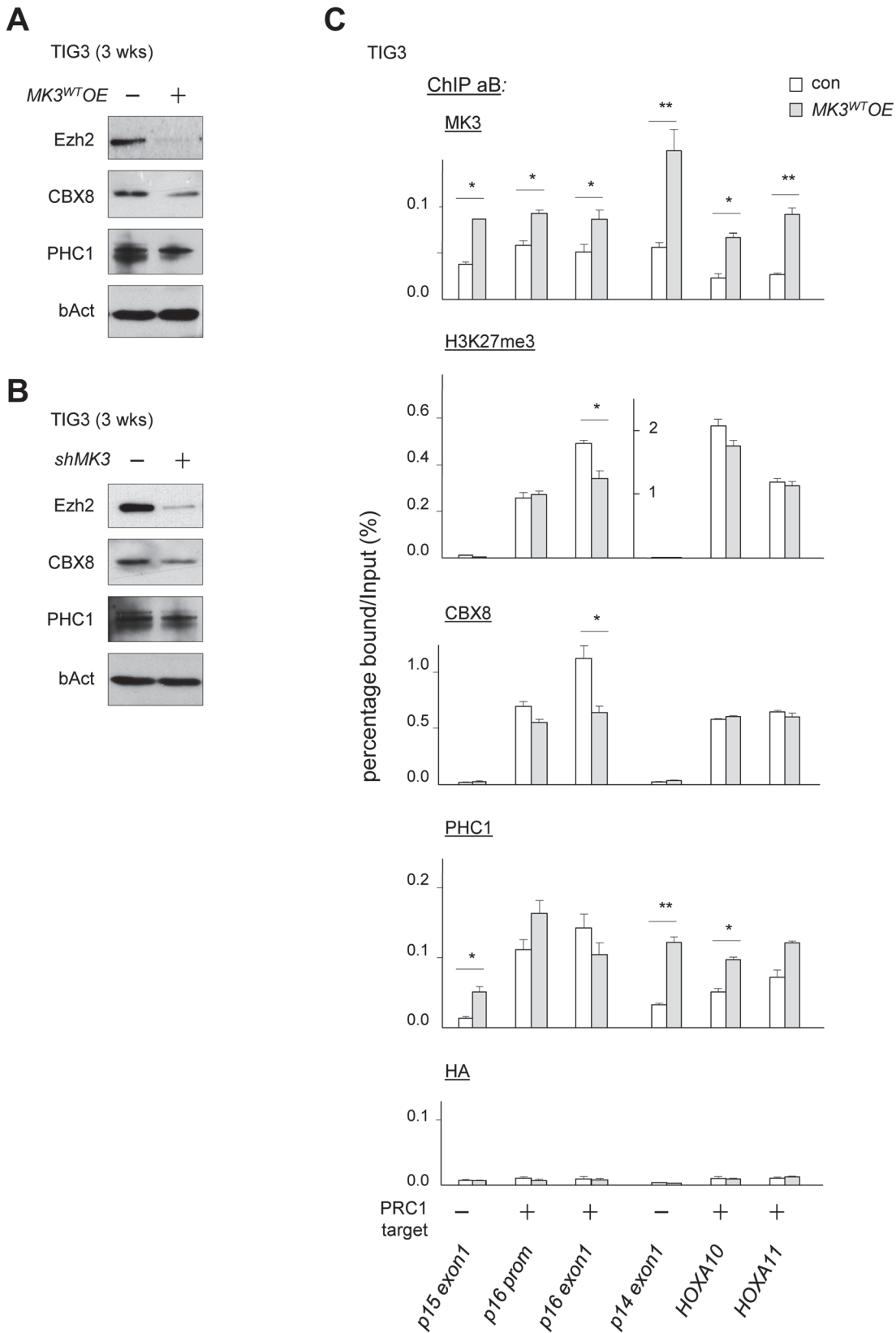


Fig 3. Functional links between MK3 and PRC in proliferative life span. (A) Expression levels of the PRC proteins EZH2, CBX8 and PHC1 in senescing TIG3/*MK3^{WT}OE* cells at ± 3 –4 weeks post-transduction; loading control b-Actin (bAct). (B) Expression levels of the PRC proteins EZH2, CBX8 and PHC1 in senescing TIG3/*shMK3* cells at ± 2 –3 weeks post-transduction; loading control b-Actin (bAct). (C) Chromatin immunoprecipitation (ChIP) analysis of MK3, H3K27me3, CBX8, PHC1 enrichment in *MK3^{WT}OE* (*MK3^{WT}OE*) expressing and control (*con*) TIG3 cells; PRC1-target loci (*p16 promoter*, *p16exon1*, *HOXA10*, *HOXA11*) and non-target loci (*p15exon1*, *p14exon1*) are indicated below the figure. Enrichments are presented as percentages of total input. Negative control HA antiserum. Experiments were performed three times; results of one representative experiment are shown (statistical significance: * $p < 0.05$, ** $p < 0.01$; t-test).

doi:10.1371/journal.pone.0118840.g003

transduced fibroblast cultures co-expressing *Bmi1*/*MK3^{WT}* self-selected for increased BMI1 protein levels over time compared to cultures overexpressing *Bmi1* alone (Fig 4E), further supporting of a genetic interaction between MK3 and BMI1 in the context of cell proliferation. As EZH2 targets the *CDKN2A/INK4A* locus for transcriptional repression, we also examined whether EZH2 alone could rescue the MK3-induced proliferative arrest. Whereas *Bmi1* co-expression in TIG3 cells clearly reduced *MK3^{WT}OE*-induced P16^{INK4} expression in the same experiment, *EZH2OE* did not prevent MK3^{WT}-induced upregulation of cellular P16^{INK4}; instead, elevated basal P16^{INK4} expression both at the mRNA and protein levels was already detectable in control cells in TIG3/*EZH2OE* cells (S4A and S4B Fig). *Bmi1* co-expression clearly neutralized the adverse effects of *MK3^{WT}OE* on cell proliferation, the effect of *EZH2OE* on the *MK3^{WT}OE*-proliferation phenotype were inconsistent, yet never compensatory (data not shown). Taken together, the above findings support a functional genetic interaction between MK3 and BMI1/PRC1 in proliferative control of normal human fibroblasts, and suggest that EZH2/PRC2 is likely neither sufficient to bypass MK3-arrested proliferation nor to prolong proliferative lifespan.

Loss of MK3 provides a growth advantage in cancer cell models

We used the large-scale cancer genome-sequencing and expression analyses initiative *Cancer Cell Line Encyclopedia* (CCLE; <http://www.broadinstitute.org/ccle>) to assess MK3 expression in nearly 1000 cancer cell lines [32]. MK3 was relatively high expressed in various cancer cell types, among which bone, pancreatic, colorectal and endometrial cancers (S5A Fig). Conversely, MK3 showed significant focal deletion across a set of more than 3000 tumors, or its expression is low/absent in cancer cell types, including small-cell lung cancers, neuro- and medulloblastomas [32]. Although cancers of (neur)ectodermal origin tend to show low/absent MK3 expression, there was no obvious correlation between germ-layer origin and MK3 expression among the various cancer types (S5A Fig), suggesting that MK3 status is an acquired feature in tumors. When we next examined MK3 protein levels in a panel of cancer cell lines, we were able to confirm large variation in MK3 expression between different cell lines (S5B Fig); no obvious correlation was observed between MK3 and MK2 levels, in line with their distinct cellular functions [33,34]. Combined, this data points to a possible involvement of MK3 in tumorigenesis and suggests that the role of MK3 may be determined by cellular and/or genetic context.

Given its possible dual involvement in tumorigenesis, we probed cancer cell lines for effects of gain or loss of MK3 function on cell proliferation. We here focused on U-2OS osteosarcoma cells and the HeLa cervical carcinoma cells. Of note, U-2OS/*MK3^{WT}OE* cultures also showed an *MK3^{WT}OE*-induced reduction of proliferation and enhanced flat cell morphology ($9.6\% \pm 1.8$ *MK3^{WT}OE* vs. $2.3\% \pm 0.8$ con, $P < 0.001$) and expression of SA-bGal (Fig 5A, 5B and S6A Fig). HeLa/*MK3OE* cells also showed enhanced flat cell induction (data not shown). Consistent with a response resembling senescence, U-2OS/*MK3^{WT}OE* cultures showed enhanced expression of TP53 and of its transcriptional target P21^{CIP1/WAF1} (Fig 5C). Consistent with the

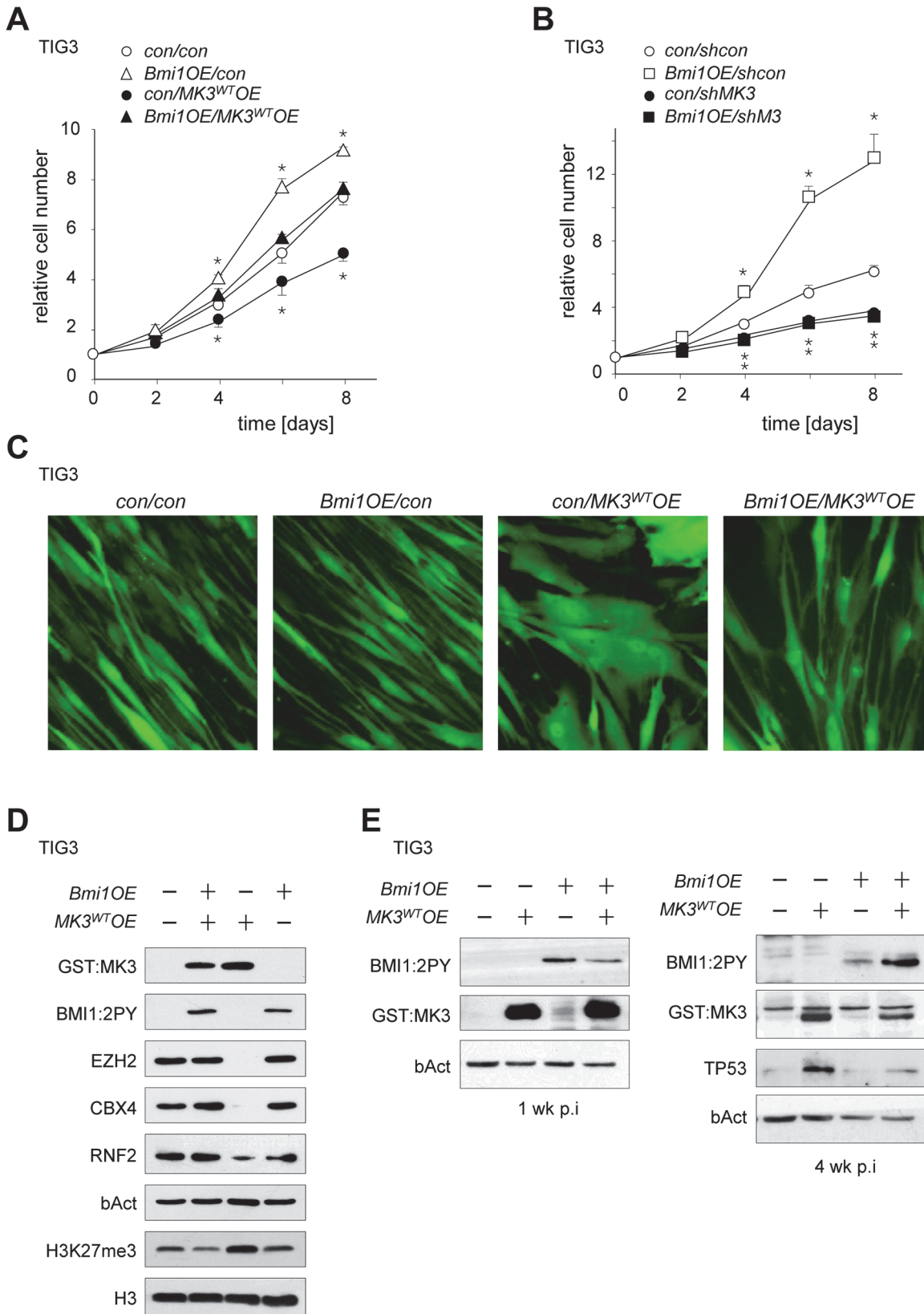


Fig 4. Functional links between MK3 and PRC in proliferative life span. TIG3 cells were sequentially transduced with either *Bmi1.ires.GFP* (*Bmi1OE*) or *GFP* (con) virus, and *MK3/puromycin* (*MK3OE*) or control *puromycin* virus (con) at 48 hrs intervals. Retroviral vectors expressing murine *Bmi1/GFP* reporter were transduced first (or empty vector control), followed by a *MK3/puromycin* resistance marker (or empty vector control). Transduction of *Bmi1OE* and control transduced cells was simultaneously carried out with the same *MK3^{WT}OE* viral preparation (or control virus) to minimize inter-experimental variation. Cells were grown on selection medium and proliferation capacity was tested \pm 2–3 weeks post-transduction. (A) Proliferation curves of normal human TIG3 fibroblasts transduced with a retroviral *MK3^{WT} overexpression* vector (*MK3^{WT}OE*; black symbols) or *shcon* vector (white symbols), in conjunction with either an empty vector control (con; circles) or a murine *Bmi1* expression vector (*Bmi1OE*; triangles). (B) Proliferation curves of normal human TIG3 fibroblasts transduced with a retroviral *MK3* knock-down vector (*shMK3*; black symbols) or *shcon* vector (white symbols), in conjunction with either an empty vector control (con; circles) or a murine *Bmi1* expression vector (*Bmi1OE*; squares). Cell counts at $t = 2$ through $t = 8$ (A, B) were normalized to cell counts at $t = 0$ for each transduced cell culture individually (see [Methods](#) section for details); statistical significance was determined by two-tailed Student's t-test and is presented relative to the empty vector control (* $p < 0.05$). (C) Comparative morphology of TIG3 cells expression *Bmi1* and/or *MK3* versus control cells as recorded by GFP fluorescent imaging \pm 3 weeks after transduction (D) Immunoblot analysis of EZH2, CBX4, RNF2 and H3K27me3 in *MK3^{WT}OE*, *Bmi1OE*, *Bmi1OE/MK3^{WT}OE* and control TIG3 cell lysates. (E) Expression analysis of BMI1, MK3, and TP53 at the indicated time points in (corresponding to experiment in [Fig 4C](#)). Cells were grown on selection medium and analysed at 1 or 4 weeks after serial transduction; expression vectors and antibodies are indicated in the figure. Early and late samples were loaded on the same gel for BMI1 analysis; corresponding sections are shown separately.

doi:10.1371/journal.pone.0118840.g004

involvement of the TP53 pathway in DNA damage response (DDR), nuclei of flat U-2OS/*MK3^{WT}OE* cells showed increased co-staining for TP53, P14^{ARF} and P21^{CIP1/WAF1} ([S6B Fig](#)). Increased replication stress is known to induce a proliferative arrest which is often associated with double strand DNA breaks (DSB). The occurrence of replication stress-associated DSB is typically associated with an initial intraS-phase arrest, as part of a DDR [[19,35,36](#)]. U-2OS/*MK3^{WT}OE* cells showed a \pm 1.5 fold increase of cells in S-phase within days after transduction ([Fig 5D](#)). To determine whether the flat cell phenotype in U-2OS/*MK3OE* cells was associated with DNA damage, we use immunofluorescence to study the occurrence of DSB by measuring phosphorylation of histone variant H2A.X (γ H2A.X) and of KAP1 phosphorylation at serine 824 (pKAP1). Double-positive γ H2A.X/pKAP1 cells were found in considerable numbers throughout U-2OS/*MK3^{WT}OE* cultures; the nuclei of enlarged flat cells were prominently stained ([Fig 5E](#)).

As the parental U-2OS and HeLa cell lines both express moderate levels of MK3 ([cf. S5B Fig](#)), we studied the effect of RNAi-mediated MK3 depletion on cell proliferation. Remarkably, both U-2OS and HeLa cells proliferated faster in the absence of MK3 ([Fig 6A](#)). Thus, in contrast to the negative effects of gain and loss of MK3 function on proliferative capacity in normal human fibroblasts, *MK3^{WT}* overexpression and ablation produce opposing effects in cancer cell models.

MK3 modulation or mutation induce signaling imbalance

The finding that proliferation capacity of U-2OS and HeLa cells was decreased in the context of *MK3OE* was unexpected. U-2OS osteosarcoma and HeLa cervical carcinoma cells both retain a “wild type” genetic status for *TP53* and *pRB* and both carry a genetically intact *CDKN2A/INK4A* locus [[37,38](#)]. Both TP53 and pRB-dependent checkpoints are, however, compromised in these cells (see [Discussion](#) section). In U-2OS cells, the *P16/INK4A* promoter is transcriptionally silenced due to CpG methylation [[38,39](#)]. HeLa cells have an intrinsically high P16^{INK4A} level; the pRB/P16^{INK4A} checkpoint is dysfunctional in these cells, however, as pRB is continuously targeted for proteolytic degradation by HPV-expressed oncoprotein. Combined with our earlier observation that changes in proliferation rate of TIG3/*MK3* kinase mutant cultures did not correspond well with TP53 and/or P16^{INK4A} levels, this prompted us to search for involvement of additional molecular mechanisms that may contribute to reduced proliferation in the context of gain or loss of MK3 function. MK3 is a downstream target of the M/SAPKs P38, JNK as well as ERK [[4](#)]; hence, MK3 acts as a convergence point of mitogenic

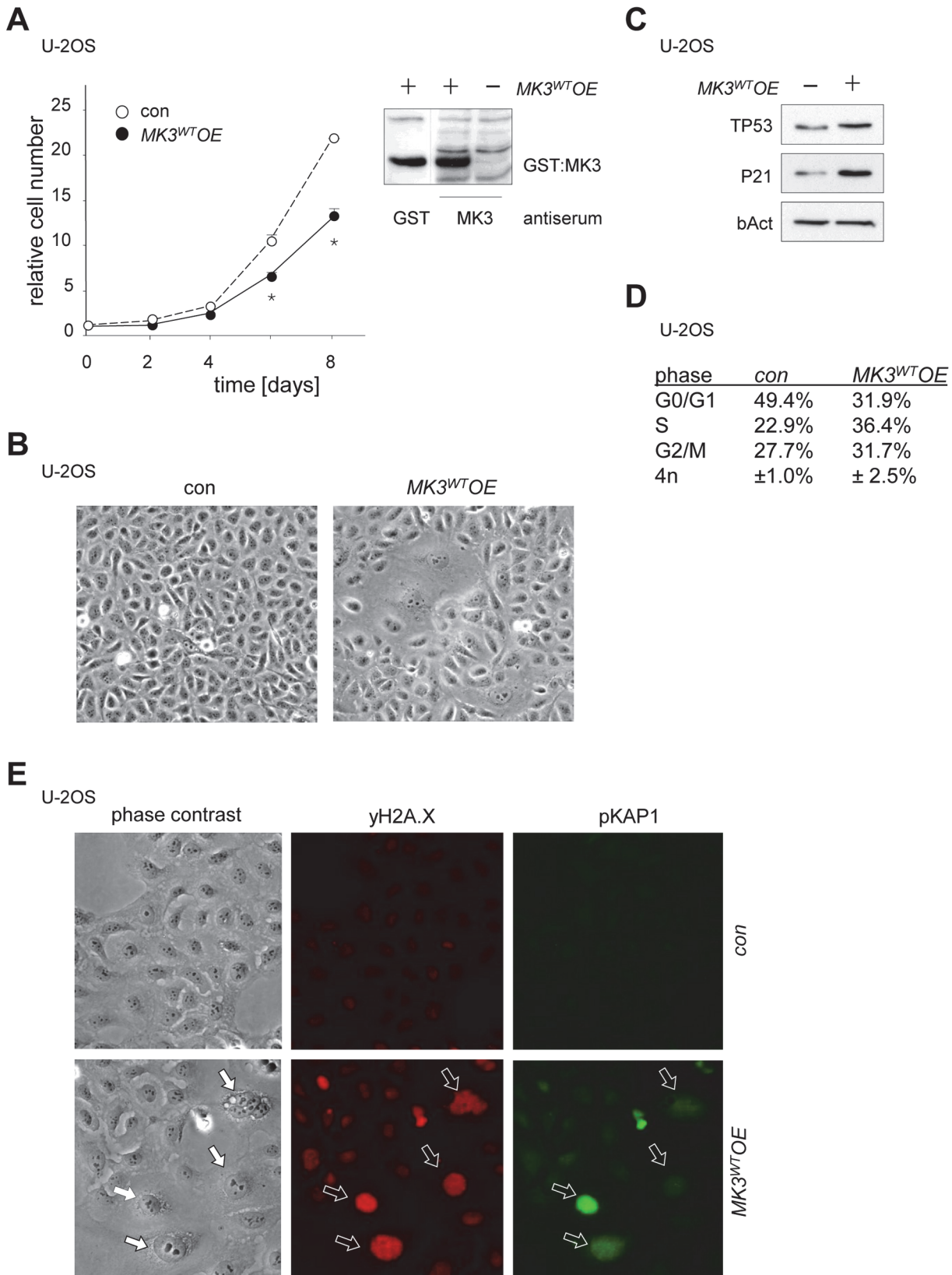


Fig 5. Proliferative regulation by MK3 in cancer cell lines. (A) Proliferation curves (left) of U-2OS cells expressing a retroviral MK3 vector ($MK3^{WT}OE$; filled circles) or an empty vector (con; open circles); overexpression of GST-MK3 ($MK3^{WT}OE$) in U-2OS cells detected with and GST or a MK3-antiserum (right panel). Cell counts at $t = 2$ through $t = 8$ were normalized to cell counts at $t = 0$ for each transduced cell culture individually (see [Methods](#) section for details); statistical significance was determined by two-tailed Student's t-test and is presented relative to the empty vector control (* $p < 0.05$). (B) Phase contrast images showing cell morphology in U-2OS/ $MK3^{WT}OE$ cells and control cells. (C) Protein expression levels of the check-point regulator proteins TP53 and p21^{CIP1/WAF1} (P21) in U-2OS/ $MK3^{WT}OE$ cells; loading control b-Actin (bAct). (D) DNA profile analysis of U-2OS/ $MK3OE$ versus control cells (4–6 days post-transduction; representative experiment). $MK3^{WT}$ overexpression elicits an intra S-phase arrest: table shows a substantially increased S-phase occupancy. (E) Immunohistochemical staining for phosphorylated H2A.X (γ H2A.X) and phosphorylated KAP1pSer824 (pKAP1; arrows) to visualize DNA damage in U-2OS/ $MK3^{WT}OE$ cultures; control (top panels) or $MK3^{WT}OE$ (bottom panels).

doi:10.1371/journal.pone.0118840.g005

and stress signaling cascades. We previously showed that gain, loss or inhibition of MK3 function affected expression levels of P38 and JNK and altered phosphorylation dynamics of ERK, P38 and JNK in response to mitogenic stimulation in U-2OS cultures [14]. As these findings pointed to an MK3-dependent M/SAPK signaling imbalance, we aimed to determine the effects of MK3 modulation in the context of cell proliferation of normal human fibroblasts and in cancer cell models. Whereas ERK and pERK (phosphorylated ERK) levels were only marginally affected under standard culturing conditions in TIG3/ $MK3^{WT}OE$ cells, JNK, P38 and phosphorylated P38 (pP38) levels were substantially increased in $MK3^{WT}OE$ fibroblasts (S7A Fig). P38 expression was sustained during prolonged culturing (S7B Fig). P38 levels were increased in $MK3^{WT}OE$ U-2OS and HeLa cultures (S7C Fig), suggesting a potential common involvement of P38 in the $MK3^{WT}OE$ -associated proliferation effects in normal and cancer cells. Conversely, yet in keeping with the increased P38 levels in $MK3OE$ cultures, P38 levels were reduced in response to MK3-depletion (*shMK3*) in both U-2OS and HeLa cancer cell lines (S7D Fig). In light of our previous finding that MK3 serves to provide negative regulatory feedback on canonical MEK/ERK signaling [14], and the current observation that P38 and JNK levels are increased in $MK3^{WT}OE$ cells, we speculated that a dysbalance in MAPK and SAPK activity could contribute to the observed effects of MK3 modulation on cell proliferation in the various cell models. In keeping with this notion, the proliferation rate of U-2OS/ $MK3^{WT}OE$ cells was negatively affected by reduction of serum concentration in a dose-dependent manner and serum deprivation (1% FCS) significantly enhanced flat cell formation in U-2OS/ $MK3^{WT}OE$ cultures (S7E Fig; cf. Fig 5B). This data supports the idea that modulation of MK3 has direct functional consequences for mitogenic responses and supports a role for signaling imbalance caused by modulation of cellular MK3 levels in normal cells as well as in cancer cells.

A recent systematic cancer genome re-sequencing effort predicted potential oncogenic driver mutations in known and novel genes [7]. Among these potentially tumorigenic MK3 variants were a number of MK3 missense mutants, among which P28S and E105A. As the effect of these mutations on MK3 function is currently unknown, we used the TIG3 model to evaluate their effect on cell proliferation, P38 and ERK levels and P38 and ERK phosphorylation. Comparable to the $MK3^{KM}$ and $MK3^{CA}$ mutant constructs, neither $MK3^{P28S}$ nor $MK3^{E105A}$ had an attenuating effect on cell proliferation at 1 week post-transduction (Fig 6B); the proliferation rate of TIG3/ $MK3^{P28S}OE$ was modestly but significantly increased over the (empty vector) control and TIG3/ $MK3^{E105A}$. In contrast, at 4 weeks post-transduction none of the *in vivo* identified MK3 mutants mimicked the negative effect of the experimental kinase mutants ($MK3^{KM}$, $MK3^{CA}$) and the non-mutated $MK3^{WT}$ kinase on proliferation (Fig 6B). Although all MK3 variants showed modestly enhanced total ERK1/2 levels, interestingly higher relative proliferation rate correlated with enhanced ERK levels (Fig 6C) in both $MK3^{P28S}$ and $MK3^{E105A}$ mutants at the 4 week time point. Under standard culturing conditions, TIG3/ $MK3^{WT}OE$, TIG3/ $MK3^{CA}OE$ and TIG3/ $MK3^{E105A}OE$ showed an sustained, increased P38 level, whereas this

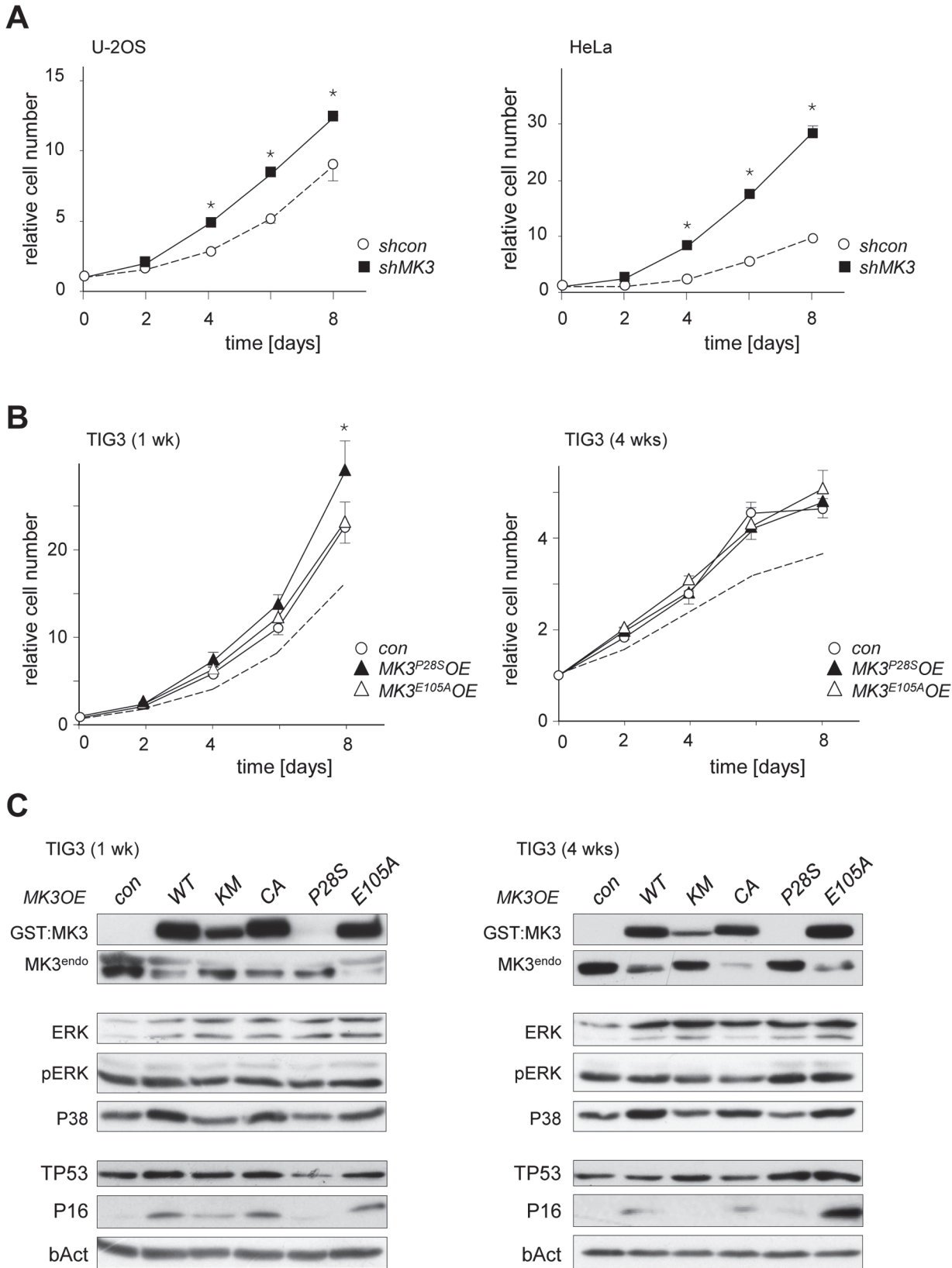


Fig 6. Modulation of MK3-levels leads to M/SAPK signalling imbalance. (A) Proliferation profiles of U-2OS/*shMK3* cells (left panel; filled squares) and HeLa/*shMK3* cells (right panel; filled squares) versus control (*shcon*; open circles). (B) Proliferation profiles of TIG3 cells expressing MK3 mutants MK3P28S (*MK3^{P28S}OE*; filled triangles) or MK3E105A (*MK3^{E105A}OE*; open triangles) at 1 week post-transduction (left panel) and 4 weeks post-transduction (right panel). The dotted lines in the graphs represent the MK3WT proliferation profiles, as depicted in S2A Fig. Cell counts at $t = 2$ through $t = 8$ (A, B) were normalized to cell counts at $t = 0$ for each transduced cell culture individually (see Methods section for details); statistical significance was determined by two-tailed Student's t-test and is presented relative to the empty vector control (* $p < 0.05$). (C) Protein expression profiles of GST-tagged MK3 (GST:MK3), endogenous MK3 (MK3^{endo}), ERK, phosphorylated ERK (pERK) P38, TP53 and p16^{INK4A} (P16) in TIG3 cells at indicated timepoints post-transduction (corresponding to Fig 4B); loading controls: b-Actin (bAct).

doi:10.1371/journal.pone.0118840.g006

effect was less clear in the TIG3/*MK3^{KM}OE* and TIG3/*MK3^{P28S}OE*; the total P38 level in the latter cells seemed slightly lower at 4 weeks post-transduction (Fig 6C). In line with the earlier noted lack of correlation between proliferation characteristics and TP53 and/or P16^{INK4A} levels, TP53 levels were highest at 4 weeks post-transduction in the cells that had the highest relative proliferation rate. Similarly, absolute P16^{INK4A} levels were highest in TIG3/*MK3^{E105A}OE* cultures (Fig 6C). We previously established that gain, loss or inhibition of MK3 function resulted in abnormal mitogenic signalling as a result of altered phosphorylation dynamics of MEK/ERK [14]. We here show that mitogenic stimulation (*i.e.* serum starvation/serum stimulation), P38 levels and phosphorylation dynamics appeared dependent on the MK3 variant expressed. P38 levels were elevated in all TIG3/*MK3^{WT}OE* cultures, irrespective of MK3 type, which is suggestive of a MK3-kinase activity independent effect (S8A and S8B Fig). TIG3/*MK3^{WT}OE*, TIG3/*MK3^{CA}OE* and TIG3/*MK3^{E105A}OE* showed more intense P38 phosphorylation compared to TIG3/*MK^{KM}OE* and TIG3/*MK3^{P28S}OE*; in addition, pP38 levels were still high in the former three cultures at 2 hours post-stimulation, compared to TIG3/*MK^{KM}OE* and TIG3/*MK3^{P28S}OE* (S8B Fig). Taken together the above data provides the first evidence that MK3-mutation affects cell proliferation. TIG3 fibroblasts thus provide a useful model to evaluate potential tumorigenic effects of novel MK3 mutants on cell proliferation. Our findings suggest that *MK3^{P28S}* and *MK3^{E105A}* mutants exert specific effects on M/SAPK signalling. In addition, the data support the notion that M/SAPK signalling intersects with TP53 and pRB mediated cell cycle checkpoints.

Discussion

The relevance of signaling through MK3 for cell proliferation was unknown. We here report that sustained gain or loss of MK3 induces a senescent state in normal human fibroblasts. Importantly, the MK3 overexpression-induced senescence is bypassed by co-expression of the oncoprotein BMI1, whereas the replicative senescent-like arrest induced by MK3 ablation is not. Surprisingly, *MK3^{WT}OE* overexpression also induces a significant reduction of proliferation in cancer cells, whereas loss of MK3 enhances cancer cell proliferation. In conjunction with our previous finding that modulation of cellular MK3 levels or inhibition of MK3 activity results in altered negative regulatory feedback to MEK/ERK we here show that gain or loss of MK3 function also affects P38. P38 levels appear to be increased by all MK3 variants, including a kinase-defective MK3, suggesting that this effect is independent of its catalytic activity. Interestingly, a number of potential oncogenic MK3 mutations showed distinct effects on ERK and P38 phosphorylation, and in contrast to non-mutant MK3 and MK3 kinase mutants, these mutants did not reduce proliferation capacity of TIG3 cells. Combined our observations support the idea that the effect of MK3 expression level modulation or MK3 mutant is dependent on cellular and genetic context.

Known senescence checkpoints in relation to MK3 modulation

TP53 and P21^{CIP1/WAF1} levels are increased both in *MK3*^{WT}*OE* and *shMK3* normal cells, in accordance with their pivotal role early in the senescence response [16,40]. The increased expression of P16^{INK4a} upon sustained *MK3* overexpression is in good agreement with its crucial role in establishing irreversible senescence [17,21,22]. As the cancer cell line models used herein are all known to be defective in their P14ARF/TP53 and/or p16/pRB checkpoints, the opposing responses of normal fibroblasts and cancer cells to MK3-depletion suggest an involvement of *CDKN2A/INK4A*. The observation that U-2OS proliferation is negatively affected by gain of MK3 was unexpected in light of the reported epigenetic inactivation of P16^{INK4A} in osteosarcoma cells [38,39]. Importantly, however, we show in the present and a previous study [8] that P14^{ARF} is induced in senescent U-2OS/*MK3*^{WT}*OE*, which, like P16^{INK4A}, is associated with replication checkpoints in human cells [23,41]. Of note, MK2 was recently suggested to control murine haematopoietic stem-cell renewal through P19^{ARF} [42]. Although the mechanism by which *CDKN2A/INK4A* expression in U-2OS/*MK3*^{WT}*OE* cells is activated remains elusive at this time, our findings suggests that P14^{ARF} may be part of the anti-proliferative response in *MK3*^{WT}*OE* cells. In addition, TP53 is induced by *MK3*^{WT}*OE* in both cancer cell lines. Even though P14^{ARF} is known to stabilize TP53 [43], we cannot formally rule out mutually independent roles for TP53, P14^{ARF} and P21^{CIP1/WAF1} in MK3-dependent proliferative control; such independent roles have been reported [44,45].

MK3 modulation and M/SAPK signaling imbalance

Our previous and current data shows that modulation of MK3 levels causes an imbalance in mitogenic and stress signaling: we find that SAPK P38 and JNK levels are increased in cells overexpressing MK3, whereas loss of MK3 correlates with reduced P38. We recently showed that MK3 controls SAPKs at multiple levels (*i.e.* JNK and P38 expression/stabilization) and that MK3 inhibition increased pERK levels in human fibroblasts, which correlated with aberrant expression of immediate early genes (*IEG*; *e.g.* *ATF3*, *EGR1*) [14]. The finding that MK3 affects P38 and ERK also agrees well with the fact that we established genetic interaction between *dMK2* and *rolled* (*dERK*) and *dP38* in *Drosophila* [14]. MK3 was shown to be targeted by all three canonical M/SAP-kinases [4], which uniquely positions MK3 at the convergence point of potentially conflicting signalling input. We here provide evidence that MK3-overexpression or ablation changes signaling through MAPK and SAPK, and has profound effects on proliferative control both in normal and cancer cell lines, positioning MK3 function both up- and down-stream of M/SAPKs, likely as part of regulatory feedback loops. The involvement of MAPKs and SAPKs in cell proliferation and proliferative life span is well documented [46,47]. Immediate-early response genes represent a standing response mechanism to a variety of triggers; their activation is closely linked to M/SAPK and MK action [48–51]. Our previous studies suggest that altered M/SAPK signalling to IEGs in the context of altered MK3 function plays a vital role in mitogenic and thereby potentially in oncogenic responses [14]. Analogously, the outcome of oncogenic signalling imbalance was reported to be dependent on critical threshold expression levels of the IEG N-MYC and, equally relevant, on the cells' intrinsic (*i.e.* genetic) state and its microenvironment [52]. Similarly, tumor suppressor function has been proposed to involve dosage and context, rather than *all-or-none* type effects [53]. As holds true for M/SAPKs, relative concentrations of MK2, MK3, and MK5 and cellular context have been proposed to dictate protein-protein interactions and thus signalling events and outcome [2,3,49].

MK3 in tumorigenesis

We used the Cancer Cell Line Encyclopedia (CCLE) to assess MK3 expression in numerous cancer cell lines [32]. This survey revealed that MK3 is relatively highly expressed in various cancer cell types whereas its expression is low/absent in other cancer cell types. *MK3* was originally proposed as a potential tumor-suppressor gene (TSG), as it located in chromosomal region 3p21.3, which frequently carries deletions in cancer. Of interest, *MK3* was recently suggested to harbour potentially oncogenic (driver) mutations, in contrast to *MK2* [7]; these included a series of missense mutations: P28S, E105A and D276Y. The P28S mutation occurs N-terminally to a predicted P-loop (AA 52–57) and the ATP-binding pocket (AA 71–77) at a position which may be conserved between MK2 and MK3 as part of a relatively proline-rich area. The E105A mutation occurs in a group of relatively polar adjacent amino acids, in between the ATP-binding pocket and two regulatory threonines (T201/T313), which constitutively activate MK3 when mutated (TT>EE in MK3^{CA}). The D276Y occurs in between the aforementioned regulatory threonines. In the current study we used our normal diploid human fibroblast model to read out effects of such two of these mutations on M/SAPK signalling and cell proliferation. Although the exact role of these mutations in tumorigenesis awaits further analysis, our observations suggest that the MK3^{P28S} and MK3^{E105A} affect cell proliferation and M/SAPK cell signalling via distinct mechanisms compared to MK3^{WT}. Expression of both MK3 mutants correlates with a relatively higher pERK level compared to MK3^{WT} or MK3 kinase mutants (KM or CA). Although both novel mutants enhance P38 signalling (level and phosphorylation), and prolonged expression of the MK3^{E105A} form correlates with relatively high P16^{INK4A} expression, neither of the two missense mutants exerts a proliferative disadvantage relative to empty vector control transduced TIG3 cells. The MK3^{E105A} mutant was originally identified in an endometrial carcinoma (EC); of note endometrial cancers show a relatively high mean MK3 expression level among cancer types [32]. The MK3^{P28S} mutant was found in a glioblastoma, a rather heterogeneous cancer type in respect to MK3 expression. Although any statement on the effect of these mutations on MK3 activity would be speculative at this point, it is conceivable that such MK3 mutants result in altered subcellular MK3 interactions that tilt the balance toward mitogenic and/or survival signalling. With respect to the MK3^{P28S} variant an obvious *caveat* is its low expression level in the current study. In depth examination of their biochemical properties, their interactome and their general effect on cell biology in the absence of wild type MK3 would prove useful to fully understand the possible implications of these potential oncogenic MK3 mutations.

The highly homologous MK2 and MK3 proteins have acquired divergent cellular-context dependent functions [2,54]. MK5 (PRAK), although required for RASV12-mediated OIS, is by itself not capable of inducing senescence and is not required for damage-induced responses [55]. We find that MK3 overexpression induces a phenotype reminiscent of oncogene-induced senescence (OIS), as evidenced by accumulation of DNA damage, activation of a DNA damage response, an intraS-phase arrest accompanied by enhanced TP53/P21^{CIP1/WAF1} expression, and ultimately P16^{INK4} and SA-bGal expression and morphological alterations typical of senescent cells. Conversely, MK3 depletion provides a selective growth advantage for cancer cell lines, which fits with enhanced mitogenic signalling through MEK/ERK, and is consistent with loss of TSG function [14]. Although the consequences of MK3 modulation on proliferative life span are likely secondary to abnormal signalling and altered checkpoint activity, combined our findings suggest that both MK3 gain- or loss-of-function may contribute to tumorigenesis depending on cellular and/or genetic context.

Functional interactions between MK3 and PRC1 in checkpoint control

The MK3-induced proliferative arrest in normal fibroblasts can be overcome by BMI1 co-expression, and clearly correlates with down-regulation of *CDKN2A/P16INK4A* expression, suggesting that MK3 and PRC1 cooperatively control proliferative lifespan. The finding that BMI1 only bypasses the effects of MK3 overexpression, not of MK3 depletion in normal cells, suggests that PRC1-dysfunction (*i.e.* complex disruption, inactivation) is unlikely to provide a common PRC1-dependent mechanistic explanation for the proliferative arrest under MK3 gain or loss-of-function. Instead these findings support the involvement of additional, PRC1-independent mechanisms in MK3-mediated checkpoint and replicative lifespan control. We did not observe a bypass-effect of EZH2 overexpression in TIG3/MK3^{WT}OE cells in this study. EZH2 is implicated in *CDKN2A/INK4A* repression, in stem-cell regulation and senescence [26,31,56–60]. Although published studies and our observations show reduced local H3K27me3 marking at the *CDKN2A* locus, globally enhanced H3K27me3-chromatin association appears to correlate to physiological stress (*e.g.* replication, hypoxia, oxidation stress; unpublished observations JWV). Given the concurrent drop in EZH2 levels and the fact that it fails to bypass MK3-induced senescence, this, by inference, implicates other regulators, among which likely H3K27me3 demethylases, in senescence responses [61]. Regulation of gene expression by histone methyl transferases like EZH2 and demethylases is known to involve regulatory non-coding RNAs, functional association with DNMTs and reciprocal functional interactions with TP53 and/or P16^{INK4A} [28,62–65]. The exact role of EZH2 in bypassing senescence is as yet not clear and may depend on tumor cell type [64,66]. As transcriptional regulatory interdependency among PRC genes has been reported [9], whether or not the reduced PRC1 levels observed in this study represent a hallmark of senescence remains to be established. The combined data herein further supports a functional interaction between PRC1 and MK3. The PRC1 oncoprotein BMI1 may thus control human cell proliferation and differentiation in ways not solely dependent on INK4A, but for instance by repression of proto-oncogenes [67]. In keeping with this idea, BMI1/RAS oncogenic collaboration and RAF1-induced senescence also involve p16^{INK4A}-independent mechanisms [68,69].

Conclusion

In summary, our findings suggest that MK3 controls cell proliferation via multiple pathways, including M/SPAKs, TSGs including TP53, P21^{cip1/waf1}, *CDKN2A/INK4A* and PRC1. The effect of gain or loss of MK3 function is context dependent and is likely to be influenced by the large variation of genetic events (heterozygous and homozygous deletions, loss of heterozygosity) involving chromosome 3p and other chromosomes in cancer. Our findings provide a starting point for systematic evaluation of these effects in different cancer types. The finding that MK3-overexpression apparently reactivates dormant checkpoints in cancer cells is an important observation, as it holds the promise of identification of novel therapeutic targets and stresses the relevance of personalized anti-cancer approaches.

Methods

Cell lines and cell culture

Human U-2OS osteosarcoma cells [70] expressing the murine ecotropic receptor were kindly provided by D. Shvarts (Utrecht Medical Center, Utrecht, The Netherlands), HeLa cervical carcinoma cells [71] by M. Koritzinsky (MAASTRO, Maastricht, The Netherlands). Normal human fibroblasts BJ [72] and TIG3 [73] were obtained through collaboration; normal human TIG3 fibroblasts expressing the murine ecotropic receptor: courtesy D. Peeper (Netherlands)

Cancer Institute, Amsterdam, The Netherlands). Cells were cultured under standard conditions in medium supplemented with 10% fetal calf serum and antibiotics (100 units/ml penicillin and 100 µg/ml streptomycin; Gibco). Serum starvation: 0.05% FCS (cancer cell lines) and 0.1% (human fibroblasts) for 48 hrs. Mitogenic stimulation: supplementation of 15% FCS and 100ng/ml tetradecanoyl phorbol acetate (TPA; Sigma-Aldrich, St. Louis, MO, USA) for the indicated duration.

cDNAs and expression systems

MK3^{KM} and *MK3^{CA}* mutant cDNAs were produced by S. Ludwig (Münster, GE). The *MK3^{P28S}* and *MK3^{E105A}* mutants were generated using the QuickChange site-directed mutagenesis method (Agilent Technologies Netherlands B.V.) and sequence verified. Retroviral expression vectors were used to maximize the percentage of expressing cells and to minimize integration effects [74,75]. Retroviral vectors (pBABE-PURO, pBMN-LZRS.ires.GFP, pBMN-LZRS.ires.NEO) expressing murine *Bmi1* and human *MK3* have been described [8]. Expression vectors encoding the murine ecotropic receptor or hTERT and human HA-tagged EZH2 were kindly provided by R. Bernards (Amsterdam, The Netherlands) and T. Jenuwein (Freiburg, Germany), respectively. Criteria used for *shRNA*-sequence design and the retroviral expression system were as described before [76]. Targeting sequences are listed in [S1 Table](#). Transduced cells were selected for 1 week on 4–16 µg/ml puromycin (Sigma).

Proliferation Assays

Growth curves were standardized: to compare cell genotypes, all viral transductions (*i.e.* various expression vectors within one experiment) were performed at the same time; all cells were seeded at equal density ($\pm 20,000$ cells/cm²) in 12-multiwell plates (Greiner Bio-one) the preceding evening and allowed to adhere overnight, before the first time point was fixed ($t = 0$) and followed over time. Cells were collected at the indicated time point cells, washed twice with phosphate-buffered saline and fixed for 10 minutes with 3.7% formaldehyde at room temperature. Next, cells were rinsed 5 times with demineralized water. Cells were stained with 0.1% Chrystal violet for 30 minutes or overnight, and washed 5 times with demineralized water. Chrystal violet was extracted with 10% acetic acid and absorbance was measured spectrophotometrically at 590 nm (Benchmark, Biorad). Data points are based on triplicate measurements within one experiment. Data (cell counts at $t = 2$ to $t = 8$) were normalized to cell counts at $t = 0$ for each transduced cell culture individually. Statistical significance ($p < 0.05$) was determined by two-tailed Student's t-test and presented relative to the empty vector control. All experiments, including transductions and selections, were repeated at least three times using fresh or frozen viral stocks.

BrdU-pulse labeling & DNA profiling

TIG3 cells were pulse-labelled with 10 µM BrdU (Sigma) for 45 min. DNA of labelled methanol-fixed cells (-20°C , overnight) was denatured (0.4 mg/ml pepsin (Sigma)/ 0.1 N HCl; 30 min) and incubated (2 N HCl, 30 min, 37°C); pH was readjusted to 7–8 with 0.1 M sodium borate buffer pH 8.5. Cells were incubated with 5 µl anti-BrdU Mab (IIB5, courtesy B. Schutte, Maastricht, The Netherlands; 1–1.5 h, RT); washed and incubated with 5 µl FITC-conjugated anti-mouse Pab (rabbit-anti-mouse FITC, Dako, Glostrup, Denmark; 4°C , overnight) washed, resuspended and stained (100 µg/ml RNase, 20 µg/ml PI/ PBS, 2–3 hrs, RT, dark) immediately prior to FACS-analysis (Becton Dickinson; CellQuest software).

Immuno-histochemistry, fluorescent *in situ* hybridization (FISH), cell staining

Cells were seeded at 5–10% confluence on glass slides, infected at low MOI ($\pm 1:1$) and subjected to a selection (*i.e.* 8 (TIG3) -16 μg (U-2OS) puromycin/ml). Cells were fixed (2% formaldehyde/PBS, 10 min RT), permeabilized (0.2% Triton-X100/PBS) or directly fixed and permeabilized (100% methanol, 20 min, -20°C). Antisera were diluted in blocking buffer (5% normal goat serum, 5% FCS, 0.02% TritonX100/PBS). Polyclonal (Pab) rabbit antiserum glutathione S-transferase (GST) and monoclonal antiserum (Mab) against MK3 were kindly provided by S. Ludwig (Münster, Germany), anti-2Py-tag Mab (MMS-115R; Babco, Richmond, California); anti-p14ARF/p16 β Pab (Ab-1; LabVision corp., Fremont, California), anti-p16INKA mab (E6H4, MTM CINtec laboratories, Heidelberg, Germany), anti-p21 Pab (C-19; Santa Cruz Biotechnology, Santa Cruz, CA, USA), anti-P53 Mab (DO-7; M7001; DAKO), anti- γH2AX Mab (JBW301, 05–636, Upstate Biotechnology/Millipore), anti-pKAP1S824 Pab (A300-767A; Bethyl Laboratories, Montgomery, TX, USA). Primary Mabs were detected with goat anti-mouse TexasRed (TXRD, Southern Biotech, Birmingham, LA, USA), primary Pabs with goat-anti-rabbit fluorescein isothiocyanate (FITC, Southern Biotech). 4'-6-Diamidino-2-phenylindole (DAPI) was co-incubated with secondary conjugated antibodies to counter-stain cell nuclei. For karyotypic analysis of TIG3, U-2OS and HeLa cells ([S9 Fig](#)), interphase FISH analysis was essentially performed as described [[77,78](#)]; Urovysion probe mixture (Abbott Molecular) containing probes for the chromosome 3, 7 and 17 centromeric regions and the 9p21 locus, labelled with SpectrumRed, SpectrumGreen, SpectrumAqua and SpectrumGold, respectively, was used; cells were counter-stained with DAPI. SA-bGal assays were performed as previously described [[79](#)].

Chromatin immunoprecipitation (ChIP) assays

TIG3 cells were transduced with pBABE-puro-GST or GST-3pK and selected with 4 $\mu\text{g}/\text{ml}$ puromycin. Fixation and ChIP procedures were essentially carried out as described before [[14,57](#)]. Briefly, cross-linked fragmented chromatin samples were immuno-precipitated overnight at 4°C with antibodies against either HA (sc-805; Santa Cruz), H3K27me3 (07–449; Upstate), an equal mix of anti-CBX8 "LAST" and "GALD" [[57](#)], anti-MK3 [[4](#)] or anti-PHC1 [[80](#)]. Crosslinks were reversed overnight at 65°C followed by a 2 h digestion with RNase A and protease K. DNA fragments were recovered using QIAquick PCR purification columns (Qiagen, Hilden, Germany), according to manufacturers' instructions. Samples were eluted in 75 μl elution buffer and then further 1/5 diluted in TE buffer. Immuno-precipitated DNA was quantified by real-time qPCR. Primer sequences: [S1 Table](#).

Western analysis

Cell lysis: RIPA buffer (5 mM Benzamidine, 5 $\mu\text{g}/\text{ml}$ Antipain, 5 $\mu\text{g}/\text{ml}$ Leupeptin, 5 $\mu\text{g}/\text{ml}$ Aprotinin, 1 mM Sodium Vanadate, 10 mM Sodium Fluoride, 10 mM Pyrophosphate, 10 mM β -Glycerophosphate, 0.5 mM DTT and 1 mM PMSF). Protein concentration: BCA protein assay kit (Pierce/Thermo Fisher Scientific, Rockford, IL, USA). Proteins were immobilized on polyvinylidene fluoride (PVDF) membranes, blocked (5% non-fat dry milk/PBS/0.1% Tween-20), incubated with antibodies (4°C , overnight): beta-Actin Mab (C4, 691001, MP Biomedicals, Solon, OH, USA), CBX8 (courtesy K.Hansen, Copenhagen, Denmark), Ezh2 Mab (BD4) and p16 Mab (DCS50; courtesy A. Bracken, BRIC, Copenhagen, Denmark), histone H3 Pab (Ab1791, Abcam, Cambridge, UK), p21 Pab (C-19; Santa Cruz Biotechnology), TP53 Mab (DO-7; M7001; DAKO), anti Bmi1 Mab (F6; courtesy M. vanLohiuzen; Amsterdam, The

Netherlands), anti MK3 Mab (3pK; clone 3p8-1, S.Ludwig, Münster, Germany), MK3 Pab (2362 3pK; U.Rapp, Würzburg, Germany), H3K27me3 Pab (07–449, Upstate), 2Py-tag Mab (MMS-115R; Babco), AKT (9272, Cell Signaling, Danvers, MA, USA), EGR1 (sc-110, Santa Cruz), MK2 Pab (3042, Cell Signaling). Signals were detected on autoradiograms using enhanced chemoluminescence (ECL; Pierce).

Quantification of mRNA levels by real-time (rt) PCR

Messenger NA levels were essentially measured as previously described [14]. Briefly, total RNA was isolated using Tri-Reagent (Sigma). RNA Quantity and quality were measured on the nanodrop (Witec AG, Luzern, Switzerland. RNA (500 ng) was converted into cDNA using the iScript cDNA synthesis kit (Bio-Rad, Hercules, CA, USA). MyIQ analysis was performed on 10 ng cDNA using the qPCR iQ Custom SYBR Green Supermix (Bio-Rad) and 300 nM primer. Analysis was performed on an iCycler thermal cycler (Bio-Rad). *Cyclophilin A* was used for normalization in all experiments. Primers sequences: [S1 Table](#).

Supporting Information

S1 Fig. MK3 overexpression induces a proliferative arrest in normal human fibroblasts. (A) Representative BrdU/DNA profile of TIG3 cells expression $MK3^{WT}$ ($MK3^{WT}OE$; lower panel) or control cells (con; upper panel). Cells were analyzed for cell cycle distribution approximately 1 week after retroviral transduction and selection. (B) Quantification of relative S-phase distribution in TIG3/con and TIG3/ $MK3^{WT}OE$ cells. S-phase sub-stage was assessed based on BrdU-incorporation pattern (*i.e.* global or focal) and DAPI staining-intensity (*i.e.* dim: early S, bright: late S; lower panel): Ed: early S/BrdU-dim, Eb: early S/BrdU-bright, M: mid S, L late S (Ld: late S/BrdU-dim in bottom panel); data are expressed as percentage of the total number of BrdU-positive cells. Note: the nearly even distribution of BrdU-positive cells over the entire S-phase and the relatively low BrdU incorporation of a substantial number of TIG3/ $MK3^{WT}OE$ nuclei are both indicative of intra-S phase arrest. (C) Cell morphology of TIG3^{hTERT}/con cells (top panel) and TIG3^{hTERT}/ $MK3^{WT}OE$ cells (bottom panel); phase contrast images. (TIF)

S2 Fig. Proliferation capacity of MK3-depleted and MK3-kinase mutant TIG3 cells. (A) Proliferation profiles of TIG3/ $MK3^{KM}OE$ and TIG3/ $MK3^{CA}OE$ cells at 1 week (left panel) and ± 4 weeks post-transduction (right panel). Note: proliferation profiles for all cell genotypes depicted in graphs [S2A Fig](#) and [Fig 6B](#) were derived simultaneously: cells were synchronously retrovirally transduced, selected, expanded and plated to determine proliferation characteristics. Cell counts at $t = 2$ through $t = 8$ were normalized to cell counts at $t = 0$ for each transduced cell culture individually (see [Methods](#) section for details); statistical significance was determined by two-tailed Student's t-test and is presented relative to the empty vector control (* $p < 0.05$). (B) Protein expression profiles of GST-tagged MK3 (GST:MK3), TP53 and p16^{INK4A} (P16) in TIG3 cells at indicated time points post-transduction (corresponding to [Fig 2SA](#)); loading controls: b-Actin (bAct). Note: the Immunoblot analysis depicted is part of the analysis as presented in [Fig 6C](#). (C) Immunoblot analysis of two different short hairpin-based RNAi vectors targeting MK3 only (*shMK3*) or MK2 and MK3 simultaneously (*shMK2/3*); loading control Tubulin (Tub). (D) Representative DNA profiles (BrdU pulse-labeling and S-phase quantification by FACS) of TIG3/*shMK3* cells corresponding to [Fig 4B](#). (E) Quantification of DNA profiles (BrdU pulse-labeling and S-phase quantification by FACS) in TIG3/*shMK3* and TIG3/con cells at approximately 1 week post-transduction. (TIF)

S3 Fig. Functional interactions between MK3 and Polycomb Group proteins. (A) Morphology of cell cultures corresponding to the chromatin immunoprecipitation (ChIP) experiments (Fig 3C); phase contrast images (right panels) confirm flat cell phenotype in TIG3/MK3^{WT}OE cells at the time of harvest. (B) Real-time PCR analysis of *EZH2* and *INK4A/ARF* mRNA levels in TIG3/MK3^{WT}OE and control cells; bottom: schematic overview of human *INK4A/ARF* locus and primers used in this study. Due to overlap in mRNA sequences of *p14^{ARF}* and *p16^{INK4A}*, levels of *p16^{INK4A}* mRNA could not be directly measured by real time PCR; instead mRNA levels for *p14^{ARF}* only, and for *p14^{ARF}* + *p16^{INK4A}* were measured; *p16^{INK4A}* mRNA levels were deduced by subtraction; error bars are provided for *p14^{ARF}* and for *p14^{ARF}* + *p16^{INK4A}* measurements. (TIF)

S4 Fig. Functional interaction between MK3 and Polycomb Repressive Complex 1. (A) Analysis of P16^{INK4A} (P16) levels in control (con), HA-tagged EZH2 (HA:EZH2); 2PY-tagged BMI1 (BMI1:2PY) and GST-tagged MK3 (GST:MK3)-transduced TIG3 cells in the presence or absence of MK3^{WT}OE (GST:MK3); tubulin (tub) and histone H3 (H3) represent fractionation controls. Cytoplasmic and nuclear fractions were always loaded on the same gel for protein analysis (corresponding sections are shown separately); nuclear fractions correspond to approximately 3–4 cytoplasmic equivalents; antibodies used as indicated in figure. (B) Real-time quantitation of mRNA expression in TIG3 cells; mRNAs as indicated; note that the exon2 primer-set simultaneously detects P14^{ARF} and P16^{INK4A} (cf. S3 Fig) Expression data were normalized to cyclophilin expression; shRNA vectors used are indicated below the graph. (TIF)

S5 Fig. MK3 expression levels in normal and cancer cell lines. (A) Expression levels of MK3 mRNA based on analysis of nearly 1000 cancer cell lines (source: *Broad-Novartis Cancer Cell Line Encyclopedia*; <http://www.broadinstitute.org/ccle> [32]). (B) MK3 and MK2 protein expression in normal and cancer cell lines; TIG3: diploid human fibroblast; BJ2: diploid human fibroblast; HeLa: cervical carcinoma; U-2OS: osteosarcoma; HCT116, HT29: colorectal carcinoma; DU145: prostate carcinoma; MCF-7: breast carcinoma; U251, U87, U373 glioblastoma; A549: alveolar adeno-carcinoma; ECC1, Ishikawa: endometrial carcinoma; RL95-2 cervical adenosquamous carcinoma. (TIF)

S6 Fig. Flat cell formation in U-2OS/MK3^{WT}OE cultures. (A) Confirmation of MK3^{WT} expression in flat U-2OS/MK3^{WT}iresGFP cells (upper left panel; phase contrast) transduced with a retroviral vector co-expressing GST:MK3 and GFP (lower left panel); right panels: large flat GFP-positive U-2OS cells stain positive for SA-bGal; arrows demarcate flat cells positive for GFP (upper panel) and SA-bGal (lower panel). (B) TP53 and P14^{ARF} (P14) co-staining (left panels) or P14^{ARF} (P14) and P21^{CIP1/WAF1} (P21) co-staining (right panels) in senescent U-2OS/MK3^{WT}OE cells; nuclei were counterstained with DAPI. (TIF)

S7 Fig. Modulation of MK3-levels causes signalling imbalance. (A) Immunoblot analysis of M/SAPK (ERK, P38, JNK) and phosphorylated (pERK, pP38) levels in TIG3/MK3^{WT}OE (MK3^{WT}OE) cells versus control cells (con). (B) Immunoblot detection of sustained elevated P38 levels in TIG3/MK3^{WT}OE cells between 1 and 3 weeks post transduction. (C) Immunoblot detection of P38 levels in TIG3/MK3^{WT}OE, U-2OS/MK3^{WT}OE and HeLa/MK3^{WT}OE cells. (D) Immunoblot detection of P38, TP53, P21^{CIP1/WAF1} (P21) and p16^{INK4A} (P16) protein expression levels; loading controls: b-Actin (bAct). (E) Left: morphological changes in U-2OS/MK3^{WT}OE cultures under reduced serum conditions (1%); empty vector control cells (con). Right:

quantitation of serum-deprivation on proliferative capacity of U-2OS/MK3^{WT}OE cells (squares: 10% FCS; circles: 5% FCS; triangles: 2% FCS; open symbols: control; filled symbols: MK3OE). Indicated (brackets) is percentage growth reduction relative to control cells at each serum concentrations.

(TIF)

S8 Fig. Modulation of MK3-levels causes signalling imbalance. (A) Immunoblot analysis of P38 and phosphorylated P38 (pP38) levels in serum-starved/stimulated TIG3/MK3^{WT}OE (overexpression of wild type MK3; *WT*), TIG3/MK^{KM}OE (kinase dead MK3; *KM*), TIG3/MK3^{CA}OE (constitutively active MK3; *CA*), TIG3/MK3^{P28S}OE (potential oncogenic mutation P28S; P28S) or TIG3/MK3^{E105A}OE (potential oncogenic mutation E105A; E105A); *con* represents empty retroviral vector control cells. All cells were synchronously transduced, selected, serum starved and serum/TPA stimulated. Extracts were prepared at the indicated time points (time in minutes). Loading control: Tubulin (Tub); “t” (GST:MK3 panel) refers to longer exposure time of autoradiographic film. (B) Immunoblot analysis of P38 and pP38 levels at defined time points in the same extracts as (A); extracts of all TIG3/MK3-genotypes at defined time points were loaded on the same blot to facilitate direct quantitative comparison.

(TIF)

S9 Fig. Karyotypic analysis of used cell lines. (A) Representative FISH image of TIG3 (left), U-2OS (middle) and HeLa cells (right); detection of 9p21 (*CDKN2A/INK4A locus*, yellow) and chromosome 17 centromeres (blue); DAPI was used to counterstain nuclei. (B) Upper table depicts summary of limited karyotype analysis; lower table depicts full analysis of TIG3 (n = 67; >98% diploid), U-2OS (n = 102; mixed polyploidy) and HeLa (n = 100; >90% triploidy at all loci investigated) nuclei for centromeres of chromosome 3, 7 and 17 and 9p21.

(TIF)

S1 Table. Primers used for ChIP and mRNA expression analysis.

(DOCX)

Acknowledgments

We thank many colleagues for research materials and support of this study (please refer to *Methods* section). We thank U.R. Rapp, F. Peronnet, R. Sverdlov and J. Geraedts for critically reading the manuscript and members of the B.G. Wouters group and Molecular Genetics department for helpful discussions, A.M. Ruland for technical support.

Author Contributions

Conceived and designed the experiments: PP HECN DN YT BGW JWV. Performed the experiments: PP HECN VEHD JS FS JV CG IP SJJB EJS. Analyzed the data: PP HECN VEHD JS FS JV CG IP SJJB EJS. Contributed reagents/materials/analysis tools: EJS YT DN. Wrote the paper: PP HECN DN BGW JWV.

References

1. Keshet Y, Seger R. The MAP kinase signaling cascades: a system of hundreds of components regulates a diverse array of physiological functions. *Methods Mol Biol.* 2010; 661: 3–38. doi: [10.1007/978-1-60761-795-2_1](https://doi.org/10.1007/978-1-60761-795-2_1) PMID: [20811974](https://pubmed.ncbi.nlm.nih.gov/20811974/)
2. Gaestel M. MAPKAP kinases—MKs—two's company, three's a crowd. *Nat Rev Mol Cell Biol.* 2006; 7: 120–130. PMID: [16421520](https://pubmed.ncbi.nlm.nih.gov/16421520/)

3. Shiryayev A, Moens U. Mitogen-activated protein kinase p38 and MK2, MK3 and MK5: menage a trois or menage a quatre? *Cell Signal*. 2010; 22: 1185–1192. doi: [10.1016/j.cellsig.2010.03.002](https://doi.org/10.1016/j.cellsig.2010.03.002) PMID: [20227494](https://pubmed.ncbi.nlm.nih.gov/20227494/)
4. Ludwig S, Engel K, Hoffmeyer A, Sithanandam G, Neufeld B, Palm D, et al. 3pK, a novel mitogen-activated protein (MAP) kinase-activated protein kinase, is targeted by three MAP kinase pathways. *Mol Cell Biol*. 1996; 16: 6687–6697. PMID: [8943323](https://pubmed.ncbi.nlm.nih.gov/8943323/)
5. Protopopov AI, Li J, Winberg G, Gizatullin RZ, Kashuba VI, Klein G, et al. Human cell lines engineered for tetracycline-regulated expression of tumor suppressor candidate genes from a frequently affected chromosomal region, 3p21. *J Gene Med*. 2002; 4: 397–406. PMID: [12124982](https://pubmed.ncbi.nlm.nih.gov/12124982/)
6. Sithanandam G, Latif F, Duh F, Bernal R, Smola U, Li H, et al. 3pK, a new mitogen-activated protein kinase-activated protein kinase located in the small cell lung cancer tumor suppressor gene region [published erratum appears in *Mol Cell Biol* 1996 Apr;16(4):1880]. *Mol Cell Biol*. 1996; 16: 868–876. PMID: [8622688](https://pubmed.ncbi.nlm.nih.gov/8622688/)
7. Greenman C, Stephens P, Smith R, Dalgliesh GL, Hunter C, Bignell G, et al. Patterns of somatic mutation in human cancer genomes. *Nature*. 2007; 446: 153–158. PMID: [17344846](https://pubmed.ncbi.nlm.nih.gov/17344846/)
8. Voncken JW, Niessen H, Neufeld B, Rennefahrt U, Dahlmans V, Kubben N, et al. MAPKAP kinase 3pK phosphorylates and regulates chromatin association of the polycomb group protein Bmi1. *J Biol Chem*. 2005; 280: 5178–5187. PMID: [15563468](https://pubmed.ncbi.nlm.nih.gov/15563468/)
9. Prezioso C, Orlando V. Polycomb proteins in mammalian cell differentiation and plasticity. *FEBS Letters*. 2011; 585: 2067–2077. doi: [10.1016/j.febslet.2011.04.062](https://doi.org/10.1016/j.febslet.2011.04.062) PMID: [21575638](https://pubmed.ncbi.nlm.nih.gov/21575638/)
10. Niessen HE, Demmers JA, Voncken JW. Talking to chromatin: post-translational modulation of polycomb group function. *Epigenetics Chromatin*. 2009; 2: 10. doi: [10.1186/1756-8935-2-10](https://doi.org/10.1186/1756-8935-2-10) PMID: [19723311](https://pubmed.ncbi.nlm.nih.gov/19723311/)
11. Simon JA, Kingston RE. Mechanisms of Polycomb gene silencing: knowns and unknowns. *Nat Rev Mol Cell Biol*. 2009; 10: 697–708. doi: [10.1038/nrm2763](https://doi.org/10.1038/nrm2763) PMID: [19738629](https://pubmed.ncbi.nlm.nih.gov/19738629/)
12. Voncken JW, Schweizer D, Aagaard L, Sattler L, Jantsch MF, van Lohuizen M. Chromatin-association of the Polycomb group protein BMI 1 is cell cycle-regulated and correlates with its phosphorylation status. *J Cell Sci*. 1999; 112: 4627–4639. PMID: [10574711](https://pubmed.ncbi.nlm.nih.gov/10574711/)
13. Sparmann A, van Lohuizen M. Polycomb silencers control cell fate, development and cancer. *Nat Rev Cancer*. 2006; 6: 846–856. PMID: [17060944](https://pubmed.ncbi.nlm.nih.gov/17060944/)
14. Prickaerts P, Niessen HEC, Mouchel-Vielh E, Dahlmans VEH, van den Akker GGH, Geijselaers C, et al. MK3 controls Polycomb target gene expression via negative feedback on ERK. *Epigenetics Chromatin*. 2012; 5: 12. doi: [10.1186/1756-8935-5-12](https://doi.org/10.1186/1756-8935-5-12) PMID: [22870894](https://pubmed.ncbi.nlm.nih.gov/22870894/)
15. Ronkina N, Kotlyarov A, Dittrich-Breiholz O, Kracht M, Hitti E, Milarski K, et al. The mitogen-activated protein kinase (MAPK)-activated protein kinases MK2 and MK3 cooperate in stimulation of tumor necrosis factor biosynthesis and stabilization of p38 MAPK. *Mol Cell Biol*. 2007; 27: 170–181. PMID: [17030606](https://pubmed.ncbi.nlm.nih.gov/17030606/)
16. Serrano M, Lin AW, McCurrach ME, Beach D, Lowe SW. Oncogenic ras provokes premature cell senescence associated with accumulation of p53 and p16INK4a. *Cell*. 1997; 88: 593–602. PMID: [9054499](https://pubmed.ncbi.nlm.nih.gov/9054499/)
17. Campisi J. Senescent cells, tumor suppression, and organismal aging: good citizens, bad neighbors. *Cell*. 2005; 120: 513–522. PMID: [15734683](https://pubmed.ncbi.nlm.nih.gov/15734683/)
18. Courtois-Cox S, Genter Williams SM, Reczek EE, Johnson BW, McGillicuddy LT, Johannessen CM, et al. A negative feedback signaling network underlies oncogene-induced senescence. *Cancer Cell*. 2006; 10: 459–472. PMID: [17157787](https://pubmed.ncbi.nlm.nih.gov/17157787/)
19. Halazonetis TD, Gorgoulis VG, Bartek J. An oncogene-induced DNA damage model for cancer development. *Science*. 2008; 319: 1352–1355. doi: [10.1126/science.1140735](https://doi.org/10.1126/science.1140735) PMID: [18323444](https://pubmed.ncbi.nlm.nih.gov/18323444/)
20. Yaswen P, Campisi J. Oncogene-Induced Senescence Pathways Weave an Intricate Tapestry. *Cell*. 2007; 128: 233–234. PMID: [17254959](https://pubmed.ncbi.nlm.nih.gov/17254959/)
21. Beausejour CM, Krtolica A, Galimi F, Narita M, Lowe SW, Yaswen P, et al. Reversal of human cellular senescence: roles of the p53 and p16 pathways. *Embo J*. 2003; 22: 4212–4222. PMID: [12912919](https://pubmed.ncbi.nlm.nih.gov/12912919/)
22. Collado M, Blasco MA, Serrano M. Cellular senescence in cancer and aging. *Cell*. 2007; 130: 223–233. PMID: [17662938](https://pubmed.ncbi.nlm.nih.gov/17662938/)
23. Campisi J. Cellular senescence: putting the paradoxes in perspective. *Current Opinion in Genetics & Development*. 2010; 21: 107–112.
24. Prieur A, Peeper DS. Cellular senescence in vivo: a barrier to tumorigenesis. *Curr Opin Cell Biol*. 2008; 20: 150–155. doi: [10.1016/j.ceb.2008.01.007](https://doi.org/10.1016/j.ceb.2008.01.007) PMID: [18353625](https://pubmed.ncbi.nlm.nih.gov/18353625/)

25. Bracken AP, Kleine-Kohlbrecher D, Dietrich N, Pasini D, Gargiulo G, Beekman C, et al. The Polycomb group proteins bind throughout the INK4A-ARF locus and are disassociated in senescent cells. *Genes Dev.* 2007; 21: 525–530. PMID: [17344414](#)
26. Kheradmand Kia S, Solaimani Kartalaei P, Farahbakhshian E, Pourfarzad F, von Lindern M, Verrijzer CP. EZH2-dependent chromatin looping controls INK4a and INK4b, but not ARF, during human progenitor cell differentiation and cellular senescence. *Epigenetics & Chromatin.* 2009; 2: 16.
27. Cao R, Zhang Y. The functions of E(Z)/EZH2-mediated methylation of lysine 27 in histone H3. *Current Opinion in Genetics & Development.* 2004; 14: 155–164.
28. Tang X, Milyavsky M, Shats I, Erez N, Goldfinger N, Rotter V. Activated p53 suppresses the histone methyltransferase EZH2 gene. *Oncogene.* 2004.
29. Dietrich N, Bracken AP, Trinh E, Schjerling CK, Koseki H, Rappsilber J, et al. Bypass of senescence by the polycomb group protein CBX8 through direct binding to the INK4A-ARF locus. *Embo J.* 2007; 26: 1637–1648. PMID: [17332741](#)
30. Gil J, Peters G. Regulation of the INK4b-ARF-INK4a tumour suppressor locus: all for one or one for all. *Nat Rev Mol Cell Biol.* 2006; 7: 667–677. PMID: [16921403](#)
31. Isono K, Fujimura Y, Shinga J, Yamaki M, J OW, Takihara Y, et al. Mammalian polyhomeotic homologues phc2 and phc1 act in synergy to mediate polycomb repression of hox genes. *Mol Cell Biol.* 2005; 25: 6694–6706. PMID: [16024804](#)
32. Barretina J, Caponigro G, Stransky N, Venkatesan K, Margolin AA, Kim S, et al. The Cancer Cell Line Encyclopedia enables predictive modelling of anticancer drug sensitivity. *Nature.* 2012; 483: 603–607. doi: [10.1038/nature11003](#) PMID: [22460905](#)
33. Ehlting C, Ronkina N, Bohmer O, Albrecht U, Bode KA, Lang KS, et al. Distinct functions of the mitogen-activated protein kinase-activated protein (MAPKAP) kinases MK2 and MK3: MK2 mediates lipopolysaccharide-induced signal transducers and activators of transcription 3 (STAT3) activation by preventing negative regulatory effects of MK3. *J Biol Chem.* 2011; 286: 24113–24124. doi: [10.1074/jbc.M111.235275](#) PMID: [21586572](#)
34. Kotlyarov A, Yannoni Y, Fritz S, Laass K, Telliez JB, Pitman D, et al. Distinct cellular functions of MK2. *Mol Cell Biol.* 2002; 22: 4827–4835. PMID: [12052889](#)
35. Di Micco R, Fumagalli M, d'Adda di Fagagna F. Breaking news: high-speed race ends in arrest—how oncogenes induce senescence. *Trends in Cell Biology.* 2007; 17: 529–536. PMID: [17980599](#)
36. Mallette FA, Gaumont-Leclerc M-F, Ferbeyre G. The DNA damage signaling pathway is a critical mediator of oncogene-induced senescence. *Genes Dev.* 2007; 21: 43–48. PMID: [17210786](#)
37. Munger K, Scheffner M, Huibregtse JM, Howley PM. Interactions of HPV E6 and E7 oncoproteins with tumour suppressor gene products. *Cancer surveys.* 1992; 12: 197–217. PMID: [1322242](#)
38. Stott FJ, Bates S, James MC, McConnell BB, Starborg M, Brookes S, et al. The alternative product from the human CDKN2A locus, p14(ARF), participates in a regulatory feedback loop with p53 and MDM2. *Embo J.* 1998; 17: 5001–5014. PMID: [9724636](#)
39. Park YB, Park MJ, Kimura K, Shimizu K, Lee SH, Yokota J. Alterations in the INK4a/ARF locus and their effects on the growth of human osteosarcoma cell lines. *Cancer Genet Cytogenet.* 2002; 133: 105–111. PMID: [11943335](#)
40. Chen J, Huang X, Halicka D, Brodsky S, Avram A, Eskander J, et al. Contribution of p16INK4a and p21CIP1 pathways to induction of premature senescence of human endothelial cells: permissive role of p53. *Am J Physiol Heart Circ Physiol.* 2006; 290: H1575–1586. PMID: [16243918](#)
41. Sherr CJ. The INK4a/ARF network in tumour suppression. *Nat Rev Mol Cell Biol.* 2001; 2: 731–737. PMID: [11584300](#)
42. Schwermann J, Rathinam C, Schubert M, Schumacher S, Noyan F, Koseki H, et al. MAPKAP kinase MK2 maintains self-renewal capacity of haematopoietic stem cells. *Embo J.* 2009.
43. Pomerantz J, Schreiber-Agus N, Liegeois NJ, Silverman A, Alland L, Chin L, et al. The Ink4a tumor suppressor gene product, p19Arf, interacts with MDM2 and neutralizes MDM2's inhibition of p53. *Cell.* 1998; 92: 713–723. PMID: [9529248](#)
44. Rowland BD, Peeper DS. KLF4, p21 and context-dependent opposing forces in cancer. *Nat Rev Cancer.* 2006; 6: 11–23. PMID: [16372018](#)
45. Sherr CJ. Divorcing ARF and p53: an unsettled case. *Nat Rev Cancer.* 2006; 6: 663–673. PMID: [16915296](#)
46. Debacq-Chainiaux F, Boilan E, Dedessus Le Moutier J, Weemaels G, Toussaint O. p38(MAPK) in the senescence of human and murine fibroblasts. *Adv Exp Med Biol.* 2010; 694: 126–137. PMID: [20886761](#)

47. Maruyama J, Naguro I, Takeda K, Ichijo H. Stress-activated MAP kinase cascades in cellular senescence. *Curr Med Chem*. 2009; 16: 1229–1235. PMID: [19355881](#)
48. Dunn KL, Espino PS, Drobic B, He S, Davie JR. The Ras-MAPK signal transduction pathway, cancer and chromatin remodeling. *Biochem Cell Biol*. 2005; 83: 1–14. PMID: [15746962](#)
49. Murphy LO, Blenis J. MAPK signal specificity: the right place at the right time. *Trends in Biochemical Sciences*. 2006; 31: 268–275. PMID: [16603362](#)
50. Plotnikov A, Zehorai E, Procaccia S, Seger R. The MAPK cascades: Signaling components, nuclear roles and mechanisms of nuclear translocation. *Biochimica et Biophysica Acta (BBA)—Molecular Cell Research*. 2011; 1813: 1619–1633.
51. Sng JC, Taniura H, Yoneda Y. A tale of early response genes. *Biol Pharm Bull*. 2004; 27: 606–612. PMID: [15133230](#)
52. Murphy DJ, Junttila MR, Pouyet L, Karnezis A, Shchors K, Bui DA, et al. Distinct Thresholds Govern Myc's Biological Output In Vivo. *Cancer Cell*. 2008; 14: 447–457. doi: [10.1016/j.ccr.2008.10.018](#) PMID: [19061836](#)
53. Berger AH, Knudson AG, Pandolfi PP. A continuum model for tumour suppression. *Nature*. 2011; 476: 163–169. doi: [10.1038/nature10275](#) PMID: [21833082](#)
54. Ronkina N, Kotlyarov A, Gaestel M. MK2 and MK3—a pair of isoenzymes? *Front Biosci*. 2008; 13: 5511–5521. PMID: [18508601](#)
55. Sun P, Yoshizuka N, New L, Moser BA, Li Y, Liao R, et al. PRAK is essential for ras-induced senescence and tumor suppression. *Cell*. 2007; 128: 295–308. PMID: [17254968](#)
56. Agherbi H, Gaussmann-Wenger A, Verthuy C, Chasson L, Serrano M, Djabali M. Polycomb mediated epigenetic silencing and replication timing at the INK4a/ARF locus during senescence. *PLoS one*. 2009; 4: e5622. doi: [10.1371/journal.pone.0005622](#) PMID: [19462008](#)
57. Bracken AP, Dietrich N, Pasini D, Hansen KH, Helin K. Genome-wide mapping of Polycomb target genes unravels their roles in cell fate transitions. *Genes Dev*. 2006; 20: 1123–1136. PMID: [16618801](#)
58. Bracken AP, Pasini D, Capra M, Prosperini E, Colli E, Helin K. EZH2 is downstream of the pRB-E2F pathway, essential for proliferation and amplified in cancer. *Embo J*. 2003; 22: 5323–5335. PMID: [14532106](#)
59. Cakouros D, Isenmann S, Cooper L, Zannettino A, Anderson P, Glackin C, et al. Twist-1 induces Ezh2 recruitment regulating histone methylation along the Ink4A/Arf locus in mesenchymal stem cells. *Molecular and cellular biology*. 2012; 32: 1433–1441. doi: [10.1128/MCB.06315-11](#) PMID: [22290439](#)
60. Itahana K, Zou Y, Itahana Y, Martinez JL, Beausejour C, Jacobs JJ, et al. Control of the replicative life span of human fibroblasts by p16 and the polycomb protein Bmi-1. *Mol Cell Biol*. 2003; 23: 389–401. PMID: [12482990](#)
61. Agger K, Cloos PA, Rudkjaer L, Williams K, Andersen G, Christensen J, et al. The H3K27me3 demethylase JMJD3 contributes to the activation of the INK4A-ARF locus in response to oncogene- and stress-induced senescence. *Genes Dev*. 2009; 23: 1171–1176. doi: [10.1101/gad.510809](#) PMID: [19451217](#)
62. Reynolds PA, Sigaroudinia M, Zardo G, Wilson MB, Benton GM, Miller CJ, et al. Tumor suppressor P16INK4A regulates polycomb-mediated DNA hypermethylation in human mammary epithelial cells. *J Biol Chem*. 2006.
63. So A-Y, Jung J-W, Lee S, Kim H-S, Kang K-S. DNA Methyltransferase Controls Stem Cell Aging by Regulating BMI1 and EZH2 through MicroRNAs. *PLoS ONE*. 2011; 6: e19503. doi: [10.1371/journal.pone.0019503](#) PMID: [21572997](#)
64. Tzatsos A, Paskaleva P, Lymperi S, Contino G, Stoykova S, Chen Z, et al. Lysine-specific demethylase 2B (KDM2B)-let-7-enhancer of zester homolog 2 (EZH2) pathway regulates cell cycle progression and senescence in primary cells. *J Biol Chem*. 2011; 286: 33061–33069. doi: [10.1074/jbc.M111.257667](#) PMID: [21757686](#)
65. Vire E, Brenner C, Deplus R, Blanchon L, Fraga M, Didelot C, et al. The Polycomb group protein EZH2 directly controls DNA methylation. *Nature*. 2005.
66. Fan T, Jiang S, Chung N, Alikhan A, Ni C, Lee CC, et al. EZH2-dependent suppression of a cellular senescence phenotype in melanoma cells by inhibition of p21/CDKN1A expression. *Molecular cancer research: MCR*. 2011; 9: 418–429. doi: [10.1158/1541-7786.MCR-10-0511](#) PMID: [21383005](#)
67. Oguro H, Yuan J, Tanaka S, Miyagi S, Mochizuki-Kashio M, Ichikawa H, et al. Lethal myelofibrosis induced by Bmi1-deficient hematopoietic cells unveils a tumor suppressor function of the polycomb group genes. *The Journal of Experimental Medicine*. 2012; 209: 445–454. doi: [10.1084/jem.20111709](#) PMID: [22351929](#)

68. Datta S, Hoenerhoff MJ, Bommi P, Sainger R, Guo W-J, Dimri M, et al. Bmi-1 Cooperates with H-Ras to Transform Human Mammary Epithelial Cells via Dysregulation of Multiple Growth-Regulatory Pathways. *Cancer Res.* 2007; 67: 10286–10295. PMID: [17974970](#)
69. Olsen CL, Gardie B, Yaswen P, Stampfer MR. Raf-1-induced growth arrest in human mammary epithelial cells is p16-independent and is overcome in immortal cells during conversion. *Oncogene.* 2002; 21: 6328–6339. PMID: [12214273](#)
70. Bruland OS, Fodstad O, Stenwig AE, Pihl A. Expression and characteristics of a novel human osteosarcoma-associated cell surface antigen. *Cancer Res.* 1988; 48: 5302–5309. PMID: [2457439](#)
71. Scherer WF, Syverton JT, Gey GO. Studies on the propagation in vitro of poliomyelitis viruses. IV. Viral multiplication in a stable strain of human malignant epithelial cells (strain HeLa) derived from an epidermoid carcinoma of the cervix. *The Journal of experimental medicine.* 1953; 97: 695–710. PMID: [13052828](#)
72. Sitte N, Merker K, Von Zglinicki T, Grune T, DAVIES KJA. Protein oxidation and degradation during cellular senescence of human BJ fibroblasts: part I—effects of proliferative senescence. *The FASEB Journal.* 2000; 14: 2495–2502. PMID: [11099467](#)
73. Baker Darren J, Weaver Robbyn L, van Deursen Jan M. p21 Both Attenuates and Drives Senescence and Aging in BubR1 Progeroid Mice. *Cell Reports.* 2013; 3: 1164–1174. doi: [10.1016/j.celrep.2013.03.028](#) PMID: [23602569](#)
74. Kinsella TM, Nolan GP. Episomal vectors rapidly and stably produce high-titer recombinant retrovirus. *HumGene Ther.* 1996; 7: 1405–1413. PMID: [8844199](#)
75. Morgenstern JP, Land H. Advanced mammalian gene transfer: high titre retroviral vectors with multiple drug selection markers and a complementary helper-free packaging cell line. *Nucleic Acids Res.* 1990; 18: 3587–3596. PMID: [2194165](#)
76. Brummelkamp TR, Bernards R, Agami R. A system for stable expression of short interfering RNAs in mammalian cells. *Science.* 2002; 296: 550–553. PMID: [11910072](#)
77. Huysentruyt CJ, Baldewijns MM, Ruland AM, Tonk RJ, Vervoort PS, Smits KM, et al. Modified UroVysion scoring criteria increase the urothelial carcinoma detection rate in cases of equivocal urinary cytology. *Histopathology.* 2011; 58: 1048–1053. doi: [10.1111/j.1365-2559.2011.03859.x](#) PMID: [21707706](#)
78. Speel EJ, Schutte B, Wiegant J, Ramaekers FC, Hopman AH. A novel fluorescence detection method for in situ hybridization, based on the alkaline phosphatase-fast red reaction. *J Histochem Cytochem.* 1992; 40: 1299–1308. PMID: [1506667](#)
79. Dimri GP, Lee X, Basile G, Acosta M, Scott G, Roskelley C, et al. A biomarker that identifies senescent human cells in culture and in aging skin in vivo. *Proc Natl Acad Sci U S A.* 1995; 92: 9363–9367. PMID: [7568133](#)
80. Takihara Y, Tomotsune D, Shirai M, Katoh-Fukui Y, Nishii K, Motaleb MA, et al. Targeted disruption of the mouse homologue of the *Drosophila* polyhomeotic gene leads to altered anteroposterior patterning and neural crest defects. *Development.* 1997; 124: 3673–3682. PMID: [9367423](#)